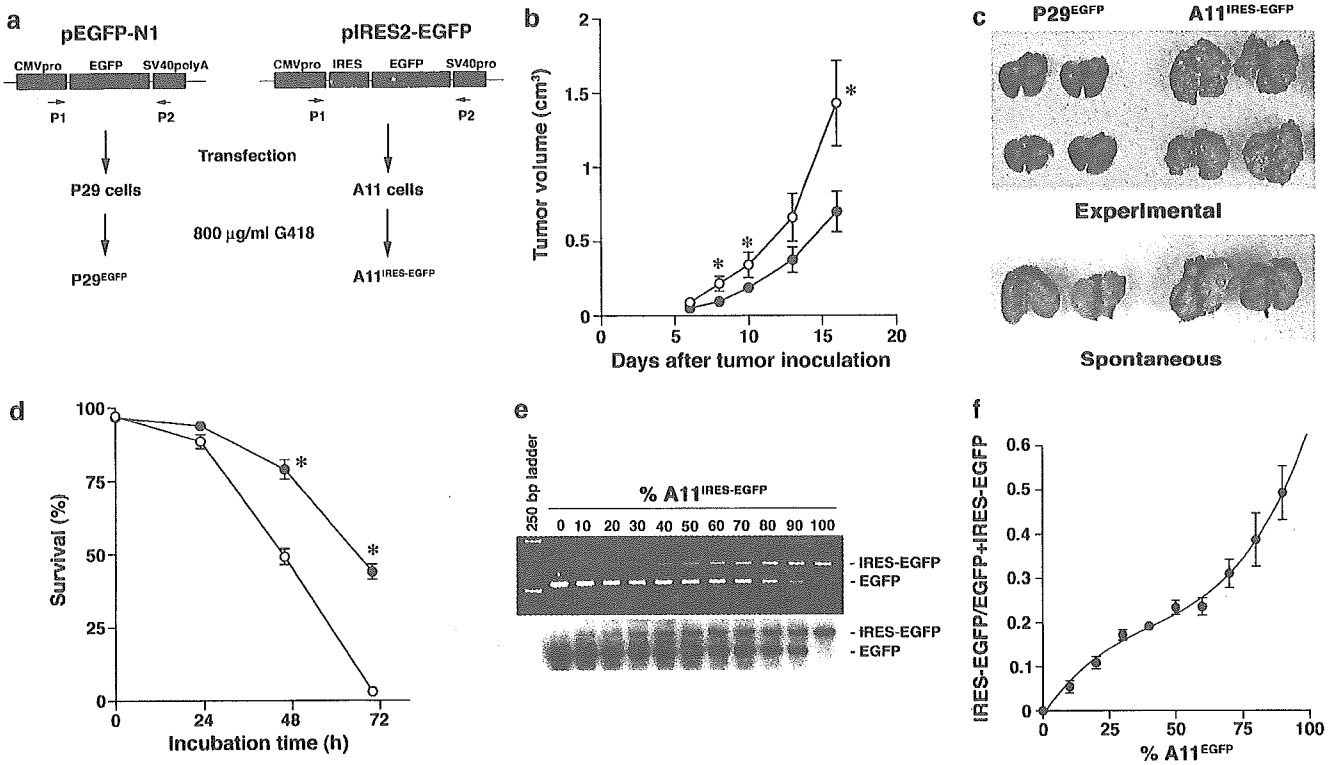

Figure 6 Establishment and properties of P29^{EGFP} and A11$^{IRES\text{-}EGFP}$ cells. (**a**) Schematic drawings of the establishment of P29^{EGFP} and A11$^{IRES\text{-}EGFP}$ cells and the primers, P1 and P2, used for PCR. (**b**) *In vivo* growth of P29^{EGFP} and A11$^{IRES\text{-}EGFP}$ cells. P29^{EGFP} (○) and A11$^{IRES\text{-}EGFP}$ cells (●) (2.5×10^5) were injected subcutaneously into C57BL/6 mice (7 mice/group). Bars; s.e.m. *Significant at $P<0.04$. (**c**) Metastatic potential of P29^{EGFP} and A11$^{IRES\text{-}EGFP}$ cells. For experimental metastasis, the cells (2×10^5 cells/mouse) were injected intravenously, and the lungs were excised 17 days after the injection. For spontaneous metastasis, the cells (2×10^5 cells/mouse) were inoculated subcutaneously, and the lungs were excised 30 days after the inoculation. (**d**) Hypoxia-induced apoptosis of P29^{EGFP} (○) and A11$^{IRES\text{-}EGFP}$ cells (●). Percentage of living cells was determined on the basis of trypan blue exclusion. Bars; s.d. of triplicate determinations. *Significant at $P<0.003$. (**e**) Ethidium bromide staining and Southern blot of PCR fragments amplified using genomic DNA extracted from mixtures of known proportions of P29^{EGFP} and A11$^{IRES\text{-}EGFP}$ cells. (**f**) A standard curve by which the percentage of A11$^{IRES\text{-}EGFP}$ cells in a mixed culture or a tumor could be calculated. The relative intensities of the bands shown in (**e**) were plotted against the known proportion of A11$^{IRES\text{-}EGFP}$ cells. Bars; s.d. of three independent experiments.

cells, respectively, treated with the same protocol was constant (Figure 7c), indicating that the integrated marker genes was stable.

Survival advantage of the high-metastatic cells in solid tumors

We next examined the proportion of A11$^{IRES\text{-}EGFP}$ cells in normoxic and hypoxic areas of solid tumors established from a 1:1 mixture of P29^{EGFP} and A11$^{IRES\text{-}EGFP}$ cells. Since P29^{EGFP} cells grew faster than A11$^{IRES\text{-}EGFP}$ cells *in vivo* (Figure 6b), the percentage of A11$^{IRES\text{-}EGFP}$ cells in both normoxic and hypoxic areas of the heterogeneous tumors should be lower than 50% if no selection of cells occurs in the tumors. We cut out EF5-negative and -positive areas (approximately total 1 mm^2) from cryosections of the tumors excised at 17 days after tumor inoculation by using laser-assisted microdissection, extracted genomic DNA, and then examined the percentage of A11$^{IRES\text{-}EGFP}$ cells in these areas as described above (Figure 8a and b). The data showed that the proportion of A11$^{IRES\text{-}EGFP}$ cells in normoxic areas decreased from the initial 50% in five out of the seven mixed tumors. However, the proportion was over 70% in #2 and #5 tumors (Figure 8b). Intriguingly, the percentage of A11$^{IRES\text{-}EGFP}$ cells in hypoxic areas was quite high in five out of the seven tumors. Overall, the proportion of A11$^{IRES\text{-}EGFP}$ cells in normoxic and hypoxic areas was 36.4 ± 26.0 and $69.0 \pm 21.0\%$, respectively ($P<0.011$). The intensity of bands corresponding to EGFP and IRES-EGFP of the cells collected from normoxic and hypoxic areas of P29^{EGFP} and A11$^{IRES\text{-}EGFP}$ tumors was constant (Figure 8c), indicating that the integrated marker genes was also stable *in vivo*. Thus, A11$^{IRES\text{-}EGFP}$ cells showed a clear survival advantage over P29^{EGFP} cells in hypoxic areas.

The loss of P29^{EGFP} cells in normoxic areas of some heterogeneous tumors (#2 and #5 tumors) suggests a possibility that a greater portion of P29^{EGFP} cells was lost in the tumors. To test this possibility, we extracted genomic DNA from the whole tumors and examined the proportion of A11$^{IRES\text{-}EGFP}$ cells. The results showed that the proportion was over 90% in #2 tumor, indicating that A11$^{IRES\text{-}EGFP}$ cells nearly overtook P29^{EGFP} cells in this tumor (Figure 8d and e). In #5 tumor, it was below 50%. This and the above results suggest that A11$^{IRES\text{-}EGFP}$

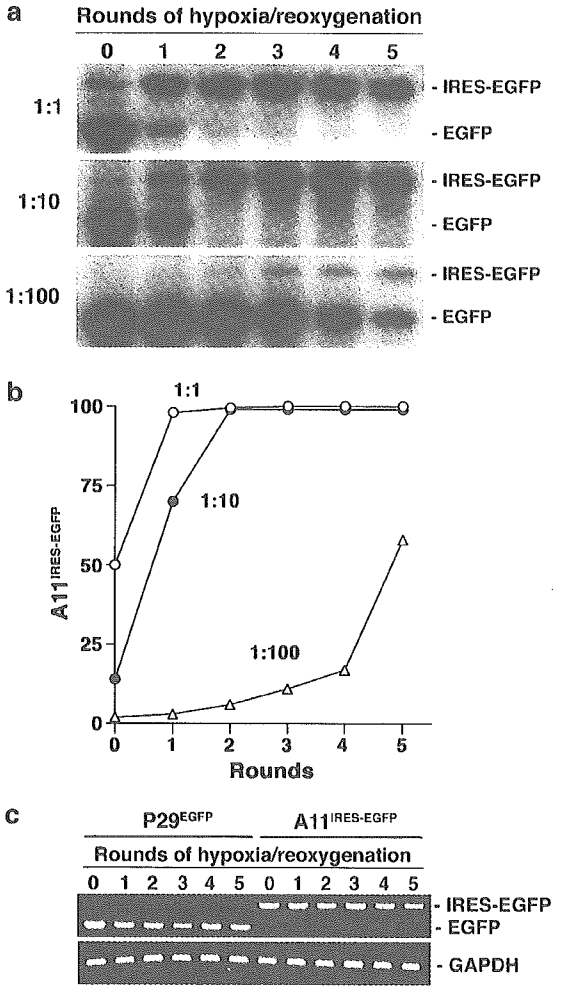

Figure 7 Hypoxia-reoxygenation selects $A11^{IRES\text{-}EGFP}$ cells in a mixed culture. (**a**) Southern blot of PCR fragments amplified using genomic DNA extracted from mixtures of $P29^{EGFP}$ and $A11^{IRES\text{-}EGFP}$ cells. $A11^{IRES\text{-}EGFP}$ were mixed with $P29^{EGFP}$ cells at a 1:1, 1:10 or 1:100 ratio and treated with multiple rounds of hypoxia-reoxygenation. (**b**) Selection of $A11^{IRES\text{-}EGFP}$ cells following hypoxia-reoxygenation treatment. The percentage of $A11^{IRES\text{-}EGFP}$ cells was calculated by the standard curve shown in Figure 6f after measuring the relative intensities of the PCR bands shown in (**a**). The data are representative of two separate experiments in which similar results were obtained. (**c**) Stability of the integrated marker genes in $P29^{EGFP}$ and $A11^{IRES\text{-}EGFP}$ cells. Ethidium bromide staining of the PCR bands is shown.

cells nearly overtook $P29^{EGFP}$ cells only in the local normoxic areas that were dissected by microdissection. The percentage of $A1^{IRES\text{-}EGFP}$ cells was over 50% in #1 and #6 tumors, suggesting that the cells were overtaking $P29^{EGFP}$ cells in these tumors. In other 3 tumors, the percentage was below 50%, indicating that selection of $A11^{IRES\text{-}EGFP}$ cells was occurring in local hypoxic areas of these tumors but was not apparent in whole tumor mass.

Discussion

The data presented here showed a close correlation between metastatic potential and the resistance to hypoxia-induced apoptosis among the cell lines with differing metastatic potential. They also showed that the high-metastatic cells are more resistant to ER stress-induced apoptosis. The hypoxia-induced apoptosis may be p53-independent, because hypoxia neither caused p53 accumulation nor induced the expressions of endogenous downstream p53 effector proteins. An apoptosis-specific expression profiling and immunoblot analyses demonstrated a correlation between the resistance to hypoxia-induced apoptosis and the expression level of Mcl-1. Downregulation of the Mcl-1 expression in A11 cells by Mcl-1 siRNA increased the sensitivity to hypoxia-induced cell death and, importantly, decreased the metastatic ability. Although there are so far few reports directly indicating the involvement of Mcl-1 in metastatic potential of tumor cells, a clinicopathological study suggested Mcl-1 as an indicator of tumor progression and prognosis in patients with gastric carcinoma (Maeta *et al.*, 2004). Therefore, Mcl-1 may be one of the factors that confer metastatic potential on at least some tumor cells.

In agreement with the previous reports (Bruick, 2000; Guo *et al*, 2001), hypoxia induced the expression of Bnip3 in all of the cell lines used in this study. Bnip3 is a mitochondrial protein and induces apoptosis independently of Apaf-1, cytochrome *c* release and caspase activation (Vande Velde *et al.*, 2000). Bcl-2 and Bcl-X_L bind to Bnip3 and inhibit apoptosis caused by the overexpression of Bnip3 (Ray *et al.*, 2000). Therefore, it is possible that Mcl-1 binds to Bnip3 and inhibits Bnip3-induced apoptosis. We preliminarily examined this possibility, and the data showed that Mcl-1 physically interacts with Bnip3 (data not shown).

There was no difference in the inducibility of ER stress- and hypoxia-inducible genes such as GADD153, GRP78 and ORP150 genes between the low- and the high-metastatic cell lines, eliminating the involvement of these genes in the difference of the sensitivity to hypoxia- and ER-stress-induced apoptosis.

The present results clearly demonstrated the survival advantage of A11 cells over P29 cells. In the mixed culture, A11 cells overtook P29 cells during several rounds of hypoxia-reoxygenation. It would be of interest to note that as the rounds of selection proceeded A11 cells progressively became more resistant to apoptosis induced by not only hypoxia but also serum starvation, glucose deprivation and anticancer drugs such as cisplatin and etoposide (not shown). Therefore, it is likely that repeated exposure to hypoxia-reoxygenation results in the selection of not merely A11 cells with original phenotype but of A11 cells with more malignant phenotype, consistent with previous reports (Kim *et al.*, 1997; Kinoshita *et al.*, 2001).

Coinciding with the *in vitro* experiments, the frequency of apoptosis was greater in the hypoxic areas of A11 tumors than in those of P29 tumors. Intriguingly, it appeared that A11 cells became a majority in the hypoxic areas of many tumor masses established from equal mixtures of P29 and A11 cells. It is of note that although we randomly excised the hypoxic areas the proportion of A11 cells in these areas was over 90% in

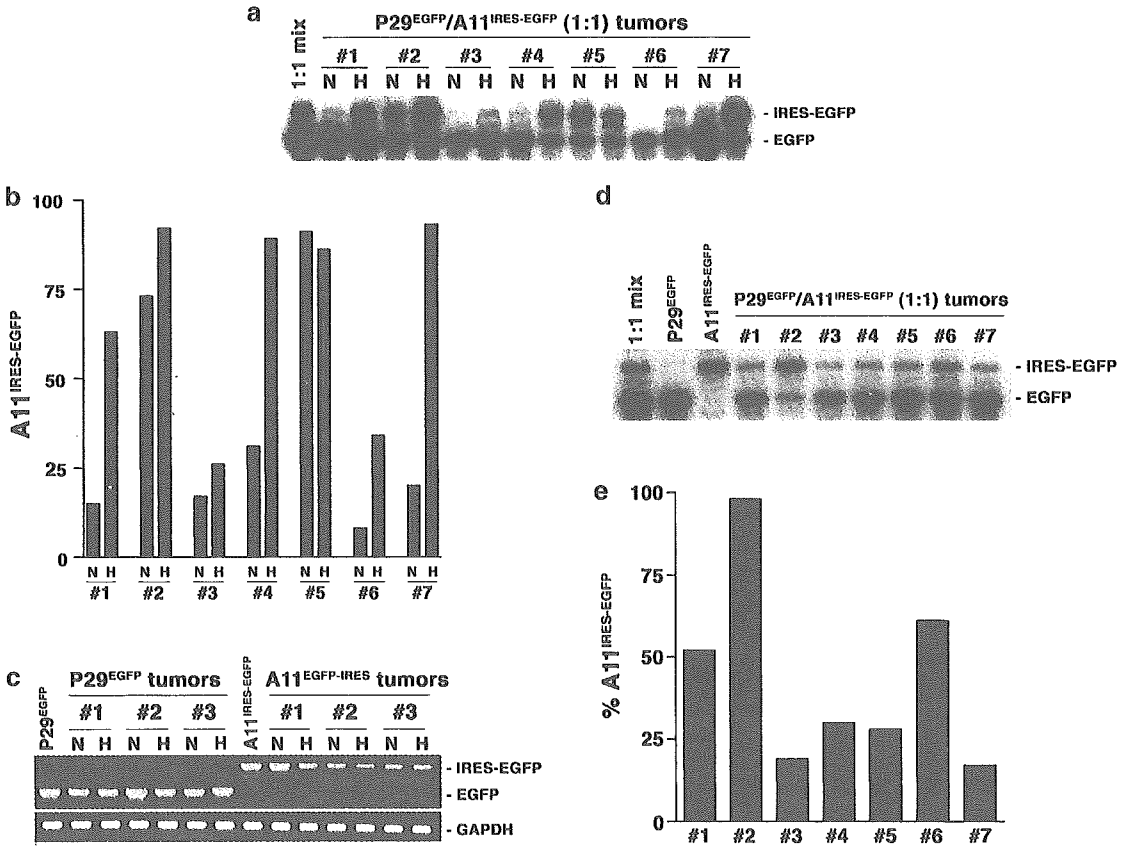

Figure 8 Proportion of $A11^{IRES\text{-}EGFP}$ cells in tumors. (**a**) Southern blot of PCR fragments amplified using genomic DNA extracted from normoxic (N) and hypoxic (H) areas in subcutaneous tumors established from equal mixtures of $P29^{EGFP}$ and $A11^{IRES\text{-}EGFP}$ cells. (**b**) The percentage of $A11^{IRES\text{-}EGFP}$ cells in normoxic (N) and hypoxic (H) areas in subcutaneous tumors. The percentage of $A11^{IRES\text{-}EGFP}$ cells was calculated by the standard curve shown in Figure 5f after measuring the relative intensities of the PCR bands shown in (**a**). (**c**) Stability of the integrated marker genes in normoxic (N) and hypoxic (H) areas of $P29^{EGFP}$ and $A11^{IRES\text{-}EGFP}$ tumors. Ethidium bromide staining of the PCR bands is shown. (**d**) Southern blot of PCR fragments amplified using genomic DNA extracted from subcutaneous tumors established from equal mixtures of $P29^{EGFP}$ and $A11^{IRES\text{-}EGFP}$ cells. (**e**) The percentage of $A11^{IRES\text{-}EGFP}$ cells in subcutaneous tumors. The percentage of $A11^{IRES\text{-}EGFP}$ cells was calculated by the standard curve shown in Figure 6f after measuring the relative intensities of the PCR bands shown in (**d**). Tumor numbers (#) correspond to those in (**a**).

several samples. This was somewhat surprising. We had expected that the proportion would vary widely from one sample to another, because the time of hypoxia influences the degree of apoptosis and EF5-binding does not tell us how long hypoxia had lasted in EF5-positive areas before excision. Nevertheless, a majority of P29 cells was commonly lost in the randomly selected hypoxic areas. One possible explanation for this is that P29 cells die more rapidly in *in vivo* hypoxic areas in which starvation of growth factors and nutrients that could act synergistically with hypoxia to induce apoptosis also occurs. We then exposed P29 and A11 cells to serum starvation (0.5% FBS) and hypoxia (0.1% O_2) simultaneously. The data showed that more than 75% of P29 cells died within 24 h while more than 70% of A11 cells survived. Thus, P29 cells are less tolerant towards severer conditions in *in vivo* hypoxic areas than A11 cells, and this might explain the rapid loss of P29 cells in hypoxic areas. Interestingly, we observed two cases out of the seven tumors in which A11 cells dominated in not only hypoxic areas but also normoxic areas. It is possible that the normoxic areas represent the ones that are reoxygenated after hypoxia. Intriguingly, in one case (#2 tumor), the proportion of A11 cells in the tumor mass was over 90%. This suggests that a majority of P29 cells died of apoptosis induced by severe hypoxia and other microenvironmental factors in the early phase of growth of this tumor, resulting in the selection of A11 cells. The degree of tumor vascularization and angiogenesis may vary from one tumor to another even if they are established from the same tumor cells, and accordingly the extent of hypoxia may differ in individual tumor. This may explain the difference in the proportion of A11 cells in each tumor.

It has been reported that hypoxia induces p53-dependent apoptosis and thus selects $p53^{-/-}$ cells (Graeber *et al.*, 1996). Our study showed that hypoxia selects for cells with reduced apoptotic potential and high-metastatic ability. This phenomenon could occur in human tumors such as cervical cancer, head and neck cancer and soft tissue sarcoma in which a correlation between hypoxia and aggressiveness or poor prognosis has been reported (Brizel *et al.*, 1996, 1997; Höckel

et al., 1996, 1999). Therefore, the data presented here may have important implications for malignant progression of tumors.

Materials and methods

Cell culture

The cell lines, P29, P34, C2, D6 and A11, established from Lewis lung carcinoma, have been characterized elsewhere (Takasu *et al.*, 1999; Koshikawa *et al.*, 2003). They were grown in Dulbecco's modified Eagle's medium (DMEM) containing 10% fetal bovine serum supplemented with 100 units/ml penicillin and 100 μg/ml streptomycin. Cells were cultured at 37°C in a humidified atmosphere with 5% CO_2 or under hypoxic conditions (ca. 0.1% O_2) generated in BBL GasPak Pouch (Becton Dickinson Microbiology Systems, Cockeysville, MA, USA). In some experiments, they were treated with tunicamycin (Sigma-Aldrich, St Louis, MO, USA), brefeldin A (WAKO Pure Chemical Industries, Ltd., Osaka, Japan), thapsigargin (Sigma-Aldrich), A23187 (Sigma-Aldrich) or vehicle alone.

Assessment of cell viability and apoptosis

Cells were seeded at a concentration of 3×10^5 cells/dish (Falcon 3002), and cell death was induced by culturing them under hypoxic conditions or in the presence of various drugs. For aerobic recovery, the cells were cultured in normoxia until they become subconfluent, thus the recovery time was different for each cell line. Cell viability was assessed by trypan blue dye exclusion. Flow cytometric analysis was performed as described previously (Takasu *et al.*, 1999) to detect cellular DNA fragmentation with a FACScan flow cytometer (Becton Dickinson, Mountain View, CA, USA). Chromatin condensation and fragmentation were visualized by staining the cells with DAPI (10 μg/ml). Annexin V and terminal deoxynucleotidyl transferase-mediated deoxyuridine triphosphate nick-end labeling (TUNEL) stainings were carried out using Annexin V-EGFP Apoptosis Detection Kit (MBL, Nagoya, Japan) and ApopTag Fluorescein *In situ* Apoptosis Detection Kit (Serologicals Corp., Norcross, GA, USA), respectively, according to the manufacturer's instructions. The fluorescence was observed under a Fluoview confocal laser microscope (Olympus, Tokyo, Japan). For clonogenic assay, cells were seeded at a concentration of 100 cells/well of six-well plates (Falcon 3046), incubated for 3 or 4 days under hypoxic ($\sim$0.1% O_2) conditions, and then allowed to grow under normoxic conditions for 8–10 days. Colonies were fixed with methanol and stained with 0.05% crystal violet.

Expression profiling of apoptosis-related genes

Expressions of apoptosis-related genes in normoxic and hypoxic P29 and A11 cells were carried out using Mouse Apoptosis GEArray Q™ series containing a panel of 96 key genes involved in apoptosis (SuperArray, Inc., Bethesda, MD, USA). Hybridization of the microarray with a biotin-16-dUTP-labeled cDNA probe and chemiluminescent detection were performed according to the manufacturer's instructions.

Northern blot analysis

Total RNA was electrophoresed on 1% agarose gel containing formaldehyde and transferred to nylon filters. Blots were hybridized with a ^{32}P-labeled mouse *Bnip3* cDNA probe that was prepared by RT–PCR.

Small interfering RNA (siRNA) transfection

Mcl-1 siRNA (Santa Cruz Biotechnologies, Inc., Santa Cruz, CA, USA) or Silencer Negative Control #1 siRNA (Ambion, Inc., Austin, TX, USA) was transfected into A11 cells with Lipofectamine 2000 (Invitrogen, Carlsbad, CA, USA) according to the manufacturer's protocol. At 3 days after transfection, the cells were subjected to immunoblot analysis for Mcl-1 expression, apoptosis assay and metastasis assay.

Immunoblot analysis

Cells were lysed in 1% Triton X-100, 1% sodium deoxycholate, 0.1% SDS, 50 mM Tris-HCl, pH 7.5, 150 mM NaCl, 1 mM PMSF and protease inhibitor cocktail (Sigma-Aldrich) or directly dissolved in SDS sample buffer. After centrifugation at 10 000 *g* for 10 min at 4°C, the supernatant was used for immunoblot analysis. Proteins were separated by SDS–PAGE under reducing conditions and transferred to a nitrocellulose membrane. The membrane was incubated with first antibodies, washed extensively with TBS-T, and then with species-appropriate HRP-conjugated secondary antibodies. The first antibodies used were anti-p53 antibody (Ab-3, Calbiochem-Novabiochem, Germany), anti-Mcl-1 antibody (Santa Cruz Biotechnology, Inc.), anti-GADD153 antibody (Santa Cruz Biotechnology, Inc.), anti-GRP78 antibody (Santa Cruz Biotechnology, Inc.), anti-ORP180 antibody (IBL, Fujioka, Japan) and anti-β-actin antibody (Sigma-Aldrich). Immunodetection was performed using the enhanced chemiluminescence system (ECL; Amersham Biosciences Corp., Piscataway, NJ, USA). The image of the bands was acquired with an imaging densitometer, and the signal intensities were analyzed with an NIH Image 1.63 software on a Machintosh computer. All signals were normalized to β-actin.

Tumor growth and metastasis assays

Cells (2×10^5 cells/mouse) were inoculated into the abdominal flank of age-matched female C57BL/6 mice (Nippon SLC, Hamamatsu, Japan). Subcutaneous tumor growth was monitored by caliper measurement of two diameters at right angles, and the tumor mass was estimated from the equation volume $= 0.5 \times a \times b^2$, where a and b are the larger and smaller diameters, respectively. For spontaneous metastasis assay, the mice were killed 30 days after tumor cell inoculation, and their lungs were removed. For experimental metastasis assay, tumor cells (2×10^5 cells/mouse) were injected intravenously, and the lungs were removed 17 days later. The lungs were fixed in Bouin's solution and the parietal metastatic nodules were counted. All animal experiments were performed in compliance with the institutional guidelines for the care and use of laboratory animals.

Immunohistochemistry

Subcutaneous tumors were excised, fixed in 10% buffered formalin and embedded in paraffin wax. Paraffin sections were cut at 6 μm thickness and mounted on the silane-coated glass slides. After routine dewaxing and rehydrating, the sections were incubated in 1 × ChemMate®Target Retrieval Solution (DakoCytomation, Glostrup, Denmark) at 121°C for 15 min and rinsed with Dulbecco's phosphate-buffered saline (DPBS). For quenching endogenous peroxidase activity, the sections were incubated in 0.3% H_2O_2 in methanol for 30 min. Thereafter, they were incubated with diluted normal goat serum for 20 min at room temperature and then incubated with anti-Mcl-1 antibody or normal rabbit IgG (4 μg/ml) diluted in ChemMate® Antibody Diluent (DaKoCytomation) containing 2% dry milk at 4°C for 16 h. Immunostaining was carried out by using VECTASTAIN® ABC Kit according to the

manufacturer's instructions. The sections were washed with DPBS and finally counterstained with hematoxylin.

Detection and microdissection of hypoxic areas in tumors
In all, 300 μl of EF5 solution (3 mg/ml) was injected intraperitoneally into mice bearing subcutaneous tumors (Inbal *et al.*, 1997). After 1 h, tumors were surgically removed and frozen in OCT compound. Cryostat sections cut at 10 μm were fixed with 4% paraformaldehyde and washed with DPBS. The sections were treated with 5% mouse serum, 20% dry milk and 0.3% Tween 20 in DPBS overnight at 4°C to block nonspecific binding sites. They were rinsed with 0.3% Tween 20 in DPBS and then incubated with Cy3-labeled monoclonal anti-EF5 antibody (ELK3-51) for 4 h at 4°C. After extensive washing with DPBS, tissue samples were observed under a confocal laser microscope or a fluorescence microscope. For detection of apoptotic cells *in vivo*, TUNEL staining was performed followed by EF5 staining. In some experiments, EF5 binding-positive (hypoxic) and adjacent EF5 binding-negative (normoxic) areas in tumor tissues were dissected using a laser-assisted microdissection system (Leica Microsystems, Tokyo, Japan).

Establishment of cells transfected with pEGFP-N1 or pIRES2-EGFP plasmid
P29 and A11 cells were transfected with pEGFP-N1 and pIRES2-EGFP (BD Biosciences Clontech, Tokyo, Japan), respectively, using Lipofectin reagent (Invitrogen, Tokyo, Japan). After selecting the transfected P29 or A11 cells in the presence of 800 μg/ml G418, a clone designated $P29^{EGFP}$ or $A11^{IRES\text{-}EGFP}$, respectively, was established. They were routinely cultured in the presence of 400 μg/ml G418.

DNA isolation, PCR and Southern blotting
Genomic DNA was extracted from $P29^{EGFP}$, $A11^{IRES\text{-}EGFP}$, mixed cells, solid tumors or microdissected sections by conventional method, treated with RNase A (10 μg/ml) and phenol extracted again. PCR was performed using 1–100 ng genomic DNA and *r*Taq DNA polymerase (TOYOBO Biochemicals, Osaka, Japan) on a Perkin Elmer GeneAmp PCR System 9700. The sense primer (P1) was 5′-AAC TCCGCCCCATTGACGC-3′ corresponding to the sequence within the CMV promoter, and the antisense primer (P2) was 5′-ACAAACCACAACTAGAATGCAG-3′ corresponding to the sequence in the SV40polyA signal. These primers were designed to amplify the EGFP sequence in pEGFP-N1 plasmid and the IRES-EGFP sequence in pIRES2-EGFP plasmid, thus yielding 1118 and 1693 bp PCR products, respectively. The PCR conditions were 94°C for 3 min, followed by 20–30 cycles of 94°C for 30 s, 55°C for 30 s and 72°C for 1 min. The resulting PCR products were electrophoresed on 1.2% agarose gels, transferred to nylon membranes and hybridized with a ^{32}P-labeled *EGFP* cDNA. The membranes were washed and radioactive intensity corresponding to the EGFP and IRES-EGFP bands was quantitated using a Fluoro Image Analyzer FLA-5000 (FUJIFILM, Tokyo, Japan). The measured percentage of $A11^{IRES\text{-}EGFP}$ cells was determined by dividing the intensity of the IRES-EGFP band by the total intensity of the EGFP plus IRES-EGFP bands. The actual percentage of $A11^{IRES\text{-}EGFP}$ cells in a mixed culture and in a tumor was determined from a standard curve established from Figure 6f.

Acknowledgements
We thank the National Cancer Institute (CTEP) for providing EF5. This work was supported in part by Grant-in-Aid from the Ministry of Health, Labour, and Welfare for Third Term Comprehensive Control Research for Cancer and from the Ministry of Education, Culture, Sports, Science and Technology.

References

Brizel DM, Scully SP, Harrelson JM, Layfield LJ, Bean JM, Prosnitz LR *et al.* (1996). *Cancer Res* **56**: 941–943.
Brizel DM, Sibley GS, Prosnitz LR, Scher RL, Dewhirst MW. (1997). *Int J Radiat Oncol Biol Phys* **38**: 285–289.
Brown JM, Giaccia AJ. (1998). *Cancer Res* **58**: 1408–1416.
Bruick RK. (2000). *Proc Natl Acad Sci USA* **97**: 9082–9087.
Bufalo DD, Biroccio A, Leonetti C, Zupi G. (1997). *FASEB J* **11**: 947–953.
Cairns RA, Kalliomaki T, Hill RP. (2001). *Cancer Res* **61**: 8903–8908.
Chaplin DJ, Hill SA. (1995). *Br J Cancer* **71**: 1210–1213.
Coquelle A, Toledo F, Stern S, Bieth A, Debatisse M. (1998). *Mol Cell* **2**: 259–265.
Dachs GU, Chaplin DJ. (1998). *Semin Radiat Oncol* **8**: 208–216.
Durand RE, Sham E. (1998). *Int J Radiat Oncol Biol Phys* **42**: 711–715.
Fernandez Y, Espana L, Manas S, Fabra A, Sierra A. (2000). *Cell Death Differ* **7**: 350–359.
Friedman AD. (1996). *Cancer Res* **56**: 3250–3256.
Glinsky GV. (1997). *Crit Rev Oncol Hematol* **25**: 175–186.
Glinsky GV, Glinsky VV. (1996). *Cancer Lett* **101**: 43–51.
Graeber TG, Osmanian C, Jacks T, Housman DE, Koch CJ, Lowe SW *et al.* (1996). *Nature* **379**: 88–91.
Graham CH, Forsdike J, Fitzgerald CJ, Macdonald-Goodfellow S. (1999). *Int J Cancer* **80**: 617–623.
Guo K, Searfoss G, Krolikowski D, Pagnoni M, Franks C, Clark K *et al.* (2001). *Cell Death Differ* **8**: 367–376.
Harris AL. (2002). *Nat Rev* **2**: 38–47.
Hill RP. (1990). *Cancer Metastasis Rev* **9**: 137–147.
Höckel M, Schlenger K, Aral B, Mitze M, Schaffer U, Vaupel P. (1996). *Cancer Res* **56**: 4509–4515.
Höckel M, Schlenger K, Höckel S, Vaupel P. (1999). *Cancer Res* **59**: 4525–4528.
Inbal B, Cohen O, Polak-Charcon S, Kopolovic J, Vadai E, Eisenbach L *et al.* (1997). *Nature* **390**: 180–184.
Kim CY, Tsai MH, Osmanian C, Graeber TG, Lee JE, Giffard RG *et al.* (1997). *Cancer Res* **57**: 4200–4204.
Kinoshita M, Johnson DL, Shatney CH, Lee YL, Mochizuki H. (2001). *Int J Cancer* **91**: 322–326.
Koshikawa N, Iyozumi A, Gassmann M, Takenaga K. (2003). *Oncogene* **22**: 6717–6724.
Kuwabara K, Matsumoto M, Ikeda J, Hori O, Ogawa S, Maeda Y *et al.* (1996). *J Biol Chem* **271**: 5025–5032.
Lord EM, Harwell L, Koch CJ. (1993). *Cancer Res* **53**: 5721–5726.
Lowe SW, Lin AW. (2000). *Carcinogenesis* **21**: 485–495.
Maeta Y, Tsujitani S, Matsumoto S, Yamaguchi K, Tatebe S, Kondo A *et al.* (2004). *Gastric Cancer* **7**: 78–84.
McConkey DJ, Greene G, Pettaway CA. (1996). *Cancer Res* **56**: 5594–5599.
Munro S, Pelham HR. (1986). *Cell* **46**: 291–300.

Piret JP, Minet E, Cosse JP, Ninane N, Debacq C, Raes M *et al.* (2005). *J Biol Chem* **280**: 9336–9344.
Ray R, Chen G, Vande Velde C, Cizeau J, Park JH, Reed JC *et al.* (2000). *J Biol Chem* **275**: 1439–1448.
Rice GC, Hoy C, Schimke RT. (1986). *Proc Natl Acad Sci USA* **83**: 5978–5982.
Russo CA, Weber TK, Volpe CM, Stoler DL, Petrelli NJ, Rodriguez-Bigas M *et al.* (1995). *Cancer Res* **55**: 1122–1128.
Semenza GL. (2000). *Crit Rev Biochem Mol Biol* **35**: 71–103.
Semenza GL. (2002). *Trends Mol Med* **8**: S62–S67.
Shtivelman E. (1997). *Oncogene* **14**: 2167–2173.
Takaoka A, Adachi M, Okuda H, Sato S, Yawata A, Hinoda Y *et al.* (1997). *Oncogene* **14**: 2871–2977.
Takasu M, Tada Y, Wang JO, Tagawa M, Takenaga K. (1999). *Clin Exp Metastasis* **17**: 409–416.
Teicher BA. (1994). *Cancer Metastasis Rev* **13**: 139–168.
Vande Velde C, Cizeau J, Dubik D, Alimonti J, Brown T, Israels S *et al.* (2000). *Mol Cell Biol* **20**: 5454–5468.
Wong CW, Lee A, Shientag L, Yu J, Dong Y, Kao G *et al.* (2001). *Cancer Res* **61**: 333–338.
Young SD, Hill RP. (1990). *J Natl Cancer Inst* **82**: 371–380.

Hypoxia-Regulated Expression of Attenuated Diphtheria Toxin A Fused with Hypoxia-Inducible Factor-1α Oxygen-Dependent Degradation Domain Preferentially Induces Apoptosis of Hypoxic Cells in Solid Tumor

Nobuko Koshikawa[1,2] and Keizo Takenaga[1]

Divisions of [1]Chemotherapy and [2]Pathology, Chiba Cancer Center Research Institute, Chiba, Japan

Abstract

Tumor cells in hypoxic areas of solid tumors are resistant to conventional chemotherapy and radiotherapy and thus are obstacles of cancer therapy. We report here the feasibility of applying hypoxia-regulated expression of diphtheria toxin A (DT-A) for killing hypoxic tumor cells. The expression vector was constructed to express DT-A fused with hypoxia-inducible factor-1α (HIF-1α) oxygen-dependent degradation (ODD) domain under the control of vascular endothelial growth factor gene promoter and contain erythropoietin mRNA-binding protein (ERBP)–binding sequence downstream of the DT-A/ODD sequence. *In vitro* ubiquitination assay showed that DT-A/ODD, but not DT-A, was ubiquitinated as efficient as HIF-1α under normoxic conditions in a von Hippel-Lindau– and oxygen-dependent manner. DT-A/ODD exhibited a comparable translation inhibitory activity to DT-A. ERBP-binding sequence was effective in stabilizing mRNA under hypoxic conditions in various cell types. Transfection of the vector expressing DT-A/ODD into high-metastatic Lewis lung carcinoma (3LL) A11 cells resulted in induction of apoptosis independently of hypoxia, probably due to its extreme toxicity. However, transfection of the vector expressing attenuated DT-A^{W153F}/ODD or DT-A^{H21A}/ODD resulted in a hypoxia-dependent induction of apoptosis. Liposomal gene transfer of the vector encoding DT-A^{W153F}/ODD induced apoptosis in hypoxic, but not in normoxic, areas of solid tumors established by A11 variant cells with higher resistance to hypoxia-induced apoptosis and inhibited the growth of hypoxic tumors established by 3LL-P29 cells. These results suggest that hypoxia-regulated expression of attenuated DT-A^{W153F}/ODD fusion protein is potentially of use for killing hypoxic tumor cells with minimizing the damage to normoxic normal tissues. (Cancer Res 2005; 65(24): 11622-30)

Introduction

In most solid tumors, hypoxic areas are generated due to shortage of blood supply (1, 2). Because tumor cells in these hypoxic areas do not divide, they are resistant to conventional chemotherapy and radiotherapy (3). To make the matters worse, *in vivo* exposure of certain tumor cells to hypoxia followed by reoxygenation results in enhancement of invasive and metastatic potential (4). Recent studies have shown that tumor cells under hypoxic conditions overexpress Met and CRCX4 chemokine receptor and respond to hepatocyte growth factor and stromal cell–derived factor-1α, respectively, resulting in the stimulation of invasiveness and chemoattraction to organs that express stromal cell–derived factor-1α (5, 6). It has also been reported that $p53^{-/-}$ transformed cells and some of high-metastatic tumor cells are more resistant to hypoxia-induced apoptosis compared with $p53^{+/+}$ cells and low-metastatic cells, respectively (7, 8). Mutations, genetic instability, DNA overreplication, and gene amplification are frequently induced in hypoxic cells (9–11). These data collectively indicate that hypoxic tumor cells exhibit more aggressive phenotype than normoxic ones and potentially become more malignant, and thus eradication of hypoxic tumor cells is inevitable to cure cancer patients.

Tumor cells in hypoxic microenvironments produce vascular endothelial growth factor (VEGF) to stimulate neoangiogenesis (12). Hepatoma cells also produce erythropoietin (Epo) in response to hypoxia (13). Hypoxic induction of VEGF and Epo is regulated at both transcriptional and posttranscriptional levels (14). Hypoxia activates the transcriptional complex termed hypoxia-inducible factor-1 (HIF-1), which is a heterodimer composed of an oxygen-regulated α subunit (HIF-1α) and a constitutively expressed β-subunit (HIF-1β/aryl hydrocarbon receptor nuclear translocator), both subunits being members of a subfamily of basic helix-loop-helix proteins that contain a conserved PAS domain (15, 16). HIF-1 binds to the hypoxia response element located upstream of the *VEGF* gene or downstream of the *Epo* gene and transactivates its expression (17). In normoxic conditions, HIF-1α is hydroxylated at two proline residues in the oxygen-dependent degradation (ODD) domain by HIF prolyl hydroxylases, recognized by the von Hippel-Lindau (pVHL)/Elongin B/Elongin C/Cul2 E3 ligase complex, and then subjected to rapid ubiquitination followed by proteasomal degradation (18, 19). When exposed to hypoxia, the activity of HIF prolyl hydroxylases is down-regulated and subsequently HIF-1α is rapidly stabilized (20, 21). The posttranscriptional regulation of *VEGF* and *Epo* mRNA involves the stabilization of the mRNA by the RNA-binding protein HuR and *Epo* mRNA-binding protein (ERBP), respectively, the binding site of which resides in the mRNA 3′-untranslated region (UTR; refs. 22, 23).

Hypoxia can be regarded as a physiologic abnormality that is restricted to the tumor; thus, it can be used as a trigger for heterologous gene expression. In fact, others and we have shown that hypoxia response element–regulated expression of prodrug-activating enzymes can sensitize hypoxic tumor cells to the corresponding prodrugs (24–27). Principally, however, this strategy is probably ineffective to quiescent tumor cells under hypoxic circumstances. Moreover, poor perfusion may limit prodrug

Requests for reprints: Keizo Takenaga, Division of Chemotherapy, Chiba Cancer Center Research Institute, 666-2 Nitona, Chuoh-ku, 260-8717 Chiba, Japan. Phone: 81-43-264-5431; Fax: 81-43-265-4459; E-mail: keizo@chiba-cc.jp.

doi:10.1158/0008-5472.CAN-05-0111

diffusion to hypoxic regions. Therefore, to kill hypoxic tumor cells that are quiescent and insensitive to conventional chemotherapeutic agents, it is desirable to use a method that ensures cell death once a heterologous gene is expressed in the cells.

Diphtheria toxin A chain (DT-A) is the component of diphtheria toxin that inhibits protein synthesis in susceptible cells. It directly binds NAD^+ and catalyzes the transfer of ADP ribose from NAD^+ to elongation factor 2, which irreversibly inhibits elongation factor 2 (28). *DT-A* gene has been considered to be applicable for cancer gene therapy (29–34). Because DT-A leads to rapid cell cycle–independent death, it might be useful to kill hypoxic tumor cells if its expression is properly regulated. However, because of its extreme toxicity, it is hard to reduce nonspecific cytotoxicity (35). Nevertheless, several strategies that limit its toxicity have been developed and those include targeted delivery of DT-A to specific cells or tissue-specific expression, such as DT-A immunotoxin (30), DT-A fused to peptide ligands for cell-specific receptor (32), and DT-A expression construct under the control of a regulatory element or tissue-specific promoter (31, 33, 34). With regard to cancer gene therapy, α-fetoprotein promoter and prostate-specific antigen promoter–regulated expression of *DT-A* gene led to selective killing of hepatocarcinoma cell lines and prostate cancer cell lines, respectively, by using a liposomal gene transfer system (33, 34). In other cases, however, although preferential killing of target tumor cells could be shown, nonspecific cytotoxicity could not be abolished due to the background expression of DT-A (35).

In the present study, we examined the feasibility of application of *DT-A* gene for killing hypoxic tumor cells. To induce hypoxia-dependent expression of DT-A, we constructed an expression vector harboring wild-type or attenuated *DT-A* gene under the control of VEGF promoter. To increase hypoxia specificity, we designed the expression vector to express DT-A fused with HIF-1α ODD domain, expecting that the fusion protein is rapidly ubiquitinated and degraded through proteasome pathway in normoxia but stabilized in hypoxia. In addition, we constructed it to express mRNA containing ERBP-binding sequence (EBBS), aiming for stabilization of the mRNA in hypoxia. We report here that expression of attenuated DT-A^{W153F}/HIF-1α ODD fusion protein driven by VEGF promoter causes efficient cell death of hypoxic tumor cells *in vitro* and *in vivo*.

Materials and Methods

Cells and Cell Culture

Highly metastatic A11 cells and low-metastatic P29 cells are derived from Lewis lung carcinoma and their characteristics are described elsewhere (25). pVHL-deficient human renal carcinoma 786-O and their transfectants stably expressing wild-type pVHL (referred herein as 786-O/VHL cells) were generously provided by Dr. Y. Nagashima (Yokohama City University School of Medicine, Yokohama, Japan). Human hepatoma HepG2 cells were obtained from Human Science Research Resources Bank (Osaka, Japan). The cells were cultured at 37°C in DMEM supplemented with heat-inactivated 10% fetal bovine serum, 100 units/mL penicillin, and 100 μg/mL streptomycin. They were also cultured under hypoxic environment (1% O_2) generated in NAPCO automatic O_2/CO_2 incubator (Precision Scientific, Chicago, IL). A11H10 cells were established after exposing A11 cells 10 times to severe hypoxia (<0.1% O_2, generated in GasPak Pouch, Becton Dickinson, Cockeysville, MD) reoxygenation cycle.

Plasmid Constructions

pVEGFpro-DT-A/ODD-EBBS expression plasmid. To avoid the effect of enhancer/promoter sequence that an expression vector usually contains for driving a drug selection marker gene, we used the backbone of pGL3-basic (Promega, Madison, MD) to construct the DT-A/ODD expression vector. First, EBBS corresponding to 117 nucleotides downstream of the stop codon of *Epo* mRNA was prepared by reverse transcription-PCR (RT-PCR) using total RNA isolated from HepG2 cells and the sense primer 5′-CCAGGTGTGTCCACCTGGGC-3′ and the antisense primer 5′-GACAGG-CTGGCGCTGAGCTG-3′. The resulting PCR product was subcloned into pGEM-T Easy vector (Promega) and the insert was cut out with *Not*I, gel-purified, and then inserted into the *Not*I site of pcDNA3 to make a plasmid pcDNA3-ERBP. Next, the nucleotide sequence of ODD domain corresponding to the amino acid residues 396 to 618 of human HIF-1α was amplified by RT-PCR using total RNA isolated from HepG2 cells and the sense primer 5′-ACAGGGGACAGATGACCAGG-3′ and the antisense primer 5′-TCAGGCGTCTTCCCAGCATG-3′. After subcloning in pGEM-T Easy vector, the insert was cut out with *Sal*I and *Xho*I, gel-purified, and ligated to the *Sal*I/*Xho*I cut pIBI-DT-A plasmid (kindly provided by Dr. Gail Harrison, University of Colorado Health Sciences Center, Denver, CO). The intrinsic stop codon TAG of *DT-A* gene was then changed to TTG by using Mutan-Express Km kit (TaKaRa Biomedicals, Osaka, Japan) and the oligonucleotide 5′-GGTCGACTCAAGAGGATCCC-3′ so that DT-A fuses with ODD in frame. The resulting plasmid was digested with *Nru*I and *Aat*I, blunt-ended by T4 DNA polymerase, and ligated to the *Eco*RV-cut pcDNA3-EBBS to make a plasmid pcDNA3-DT-A/ODD-EBBS. The resulting plasmid was digested with *Nco*I and *Xba*I, and the DT-A/ODD-EBBS cassette was gel-purified, blunt-ended, and then ligated to the *Nco*I/*Xba*I cut, blunt-ended pGL3-basic to make a plasmid pGL3-DT-A/ODD-EBBS. The VEGF promoter sequence of the phVEGF-1 plasmid (kindly provided by Dr. H. Esumi, National Cancer Center Research Institute East, Tokyo, Japan; ref. 36) was digested with *Kpn*I and *Nhe*I, gel-purified, and ligated to the *Kpn*I/*Nhe*I-cut pGL3-basic or pGL3-DT-A/ODD-EBBS, yielding a plasmid pVEGFpro or pVEGFpro-DT-A/ODD-EBBS, respectively. The plasmid-harboring attenuated DT-A, pVEGFpro-DT-A^{W153F}/ODD-EBBS, was made by changing the codon TGG to TTT, resulting in the amino acid change from tryptophan 153 to phenylalanine by using Transformer Site-Directed Mutagenesis kit (BD Sciences Clontech, Tokyo, Japan). pVEGFpro-DT-A^{H21A}/ODD-EBBS was made in a similar way by changing the codon CAC to GCC, resulting in the amino acid change from histidine 21 to alanine. All of the nucleotide sequence prepared by RT-PCR and mutagenesis were confirmed by nucleotide sequencing.

Luciferase reporter plasmid harboring erythropoietin mRNA-binding protein-binding sequence. The EBBS in pGEM-T Easy prepared as above was digested with *Eco*RI, blunt-ended, and then ligated to the pflM1 cut, blunt-ended pGL2-basic (Promega). The VEGF promoter sequence was then inserted into the *Kpn*I/*Nhe*I site of the plasmid to make a plasmid pVEGFpro-Luc-EBBS.

In vitro Ubiquitination Assay

In vitro ubiquitination assay was done as described previously (37). Briefly, DT-A and HIF-1α radiolabeled with ^{35}SPRO-MIX (Amersham Biosciences Corp., Piscataway, NJ) were prepared by *in vitro* transcription and translation of genes subcloned into pcDNA3 using the TNT T7 Quick Coupled Transcription/Translation System (Promega). To prepare cell extracts (S100 fraction), 293T cells were washed twice with ice-cold hypotonic extraction buffer [20 mmol/L Tris-HCl (pH 7.5), 5 mmol/L KCl, 1.5 mmol/L $MgCl_2$, and 1 mmol/L DTT]. After removal of the buffer, cells were disrupted in a Dounce homogenizer. Following cell lysis, crude extract was centrifuged at 10,000 × *g* for 10 minutes at 4°C. The supernatant was collected and further centrifuged at 100,000 × *g* for 4 hours at 4°C. The resulting cell extract (S100 fraction) was stored in aliquot at −80°C. Ubiquitination assays were done at 30°C in a total volume of 20 μL composed of 2.5 μL of programmed reticulocyte lysate, 83 μg of S100 fraction, 2 μL of 10 × ATP-regenerating system [20 mmol/L Tris-HCl (pH 7.5), 10 mmol/L ATP, 10 mmol/L magnesium acetate, 300 mmol/L creatine phosphate, and 0.5 mg/mL creatine phosphokinase], 1 μL of 10 mg/mL ubiquitin (Sigma-Aldrich, St. Louis, MO), or 10 mg/mL ubiquitin aldehyde (Boston Biochem, Cambridge, MA). Aliquots were removed at indicated times, mixed with SDS sample buffer, and analyzed by 12.5% SDS-PAGE followed by autoradiography.

In vitro Assay of Translation Inhibitory Activity of Diphtheria Toxin A

Translation inhibitory activities of DT-A, DT-A/ODD, and its attenuated fusion proteins were assayed as described (38) with some modifications. First, DT-A proteins were prepared by *in vitro* transcription/translation of genes subcloned into pcDNA3 using TNT T7 Quick Coupled Transcription/Translation System. Then, 1 μL of the translated DT-A protein was added to 11 μL of TNT SP6 Quick Coupled Transcription/Translation mixture containing 0.5 μg of NAD^+, 0.45 μL ^{35}SPRO-MIX, and 250 ng of luciferase SP6 control DNA (Promega). The samples were incubated for 90 minutes at 30°C and the proteins were separated on 12.5% SDS-PAGE and detected by autoradiography.

Luciferase Reporter Assay

For examining the effect of EBBS, the luciferase reporter plasmid, pVEGFpro-Luc or pVEGFpro-Luc-EBBS, was transiently transfected into cells using Lipofectin (Invitrogen Corp., Carlsbad, CA). As a control for transfection efficiency, pRL-CMV vector (Promega) was cotransfected with test plasmids. pGL2-control vector (Promega) was used as a positive control. Luciferase activity in cell extracts was assayed 48 hours posttransfection according to Dual-Luciferase reporter assay system protocols (Promega) using a luminometer (model TD-20/20, Turner Designs, Sunnyvale, CA).

RNA Extraction and Northern Blot Analysis

Total RNA was extracted with guanidinium thiocyanate from cells cultured under normoxic or hypoxic environment. Total RNA (20 μg) was electrophoresed on 1% agarose gel containing formaldehyde and transferred to nylon filters. Blots were hybridized with a ^{32}P-labeled mouse *VEGF* cDNA probe, which was prepared by the random primer method. Filters were finally washed at 50°C in 30 mmol/L NaCl, 3 mmol/L sodium citrate, and 0.1% SDS.

Assays for Apoptosis

Chromatin condensation and fragmentation were visualized by staining the cells with 4′,6-diamidino-2-phenylindole (DAPI, 10 μg/mL; ref. 8). Annexin V staining was done using Annexin V–enhanced green fluorescent protein (EGFP) apoptosis detection kit (MBL, Nagoya, Japan), according to the instructions of the manufacturer. Fluorescence was observed under a Fluoview confocal laser microscope (Olympus, Tokyo, Japan). Flow cytometric analysis was done as described previously (8) to analyze cellular DNA fragmentation with a FACScan flow cytometer (Becton Dickinson, Mountain View, CA). Cell death was monitored by trypan blue dye exclusion.

In vivo Gene Transfer and Detection of Hypoxic Areas and Apoptosis in Tumors

A11H10 cells (5×10^5 cells) were inoculated s.c. into the abdominal flank of female C57BL/6 mice (Nippon SLC, Shizuoka, Japan). Twelve days after the inoculation, when an estimated tumor volume reached ~800 mm^3, DNA/liposome complex that is composed of 40 μg of pEGFP-N1, pVEGFpro or pVEGFpro-DT-A^{W153F}/ODD-ERBP, 40 μL of DMRIE-C (Life Technologies, Tokyo, Japan), and 5 μg of MW 70,000, lysine-fixable dextran-tetramethylrhodamine conjugates (dextran-TMR, Molecular Probes, Inc., Eugene, OR) in 200 μL Opti-MEM was directly injected intratumorally. Two days after the injection, 300 μL of EF5 solution (3 mg/mL) were administered i.p. into mice bearing s.c. tumors (39). One hour later, tumors were surgically removed and frozen in optimum cutting temperature compound. Cryostat sections cut at 10 μm were fixed with 4% paraformaldehyde and washed with Dulbecco's PBS (DPBS). To detect apoptotic tumor cells, terminal deoxynucleotidyl transferase–mediated dUTP nick-end labeling (TUNEL) stainings were done on the sections using ApopTag Fluorescein *In situ* Apoptosis Detection kit (Serologicals Corp., Norcross, GA), according to the instructions of the manufacturer. The sections were then treated with 5% mouse serum, 20% dry milk, and 0.3% Tween 20 in DPBS overnight at 4°C to block nonspecific binding sites. They were rinsed with 0.3% Tween 20 in DPBS and then incubated with Cy5-labeled monoclonal anti-EF5 antibody (ELK3-51) for 4 hours at 4°C to detect hypoxic regions in the tumors. After extensive washing with DPBS, tissue samples were counterstained with Hoechst 33324 and observed under a fluorescence microscope. Images were captured using a Cool SNAP charge-coupled device camera and processed by a RS IMAGE Express image processing software (Nippon Roper, Chiba, Japan).

In vivo Gene Transfer and Tumor Growth

P29 cells (4×10^5) were inoculated s.c. into the abdominal flank of female C57BL/6 mice (10 mice per group). Ten days after the inoculation, DNA/liposome complex (12 μg of pVEGFpro or pVEGFpro-DT-A^{W153F}/ODD-ERBP and 3 μL of DMRIE-C in 200 μL of Opti-MEM) was directly injected into the tumor. The injection was done daily until the end of the experiments. Tumor growth was monitored by caliper measurement of two diameters at right angles and the tumor mass was estimated from the equation, volume = $0.5 \times a \times b^2$, where a and b are the larger and smaller diameters, respectively.

Determination of the Degree of Hypoxia in Subcutaneous Tumors

A11H10 and P29 cells (1×10^6) were inoculated s.c. into C57BL/6 mice. When tumor volumes reached ~650 mm^3, the mice were injected with EF5. Cryostat sections of the tumors were made at every 400 μm distance and stained with Cy3-labeled monoclonal anti-EF5 antibody (ELK3-51) as described above. For analyzing EF5-positive (hypoxic) areas on each section, at least five randomly selected fluorescent images were captured with a Leica fluorescence microscope system equipped with a computer. The images were transferred to the ImageJ 1.34s software and EF5-positive areas were analyzed. In this way, >100 fields (1.175 mm^2/field) were analyzed and the percentage of EF5-positive area per field was calculated.

Results

Oxygen and von Hippel-Lindau–dependent ubiquitination of DT-A/ODD fusion protein. To examine the effect of HIF-1α ODD domain on ubiquitination of DT-A/ODD fusion protein, we subjected the *in vitro* translated ^{35}S-labeled DT-A/ODD proteins to the *in vitro* ubiquitination assay. Incubation of DT-A/ODD with cell extract from 293T cells alone resulted in the appearance of a slower migrating form (Fig. 1*A*). The effect was enhanced by the addition of ATP generation system. Addition of ubiquitin resulted in a further mobility shift of these species. These results indicated that these mobility shifts were most likely due to ubiquitination of DT-A/ODD proteins. This was confirmed by a further shift of these species to high molecular weight proteins by the addition of ubiquitin aldehyde, an isopeptidase inhibitor that prevents the degradation of ubiquitin conjugates. Ubiquitination of DT-A/ODD, but not of DT-A that served as a control, proceeded as the incubation time prolonged (Fig. 1*B*), which was comparable with that of HIF-1α proteins (Fig. 1*C*). Addition of desferrioxamine, a hypoxia mimetic, to the reaction mixture inhibited DT-A/ODD ubiquitination in a dose-dependent manner (Fig. 1*D*). Furthermore, ubiquitination of the protein was more prominent in 786-O/VHL cells than in 786-O cells, although a low level of DT-A/ODD ubiquitination was apparent in 786-O cells (Fig. 1*E*). Taken together, these results indicate that DT-A/ODD, but not DT-A, is ubiquitinated dependently on oxygen and pVHL.

Effect of erythropoietin mRNA–binding protein binding sequence on the expression level of luciferase under hypoxic conditions. To examine the effect of EBBS on the expression level of a heterologous gene, we constructed luciferase reporter plasmids, pVEGFpro-Luc as a control and pVEGFpro-Luc-EBBS (Fig. 2*A*). After transient transfection of each reporter plasmid into A11 or HepG2 cells, they were exposed to hypoxia for 18 hours and then luciferase activity was measured. As shown in Fig. 2*B* and *C*, although integration of EBBS into the reporter plasmid resulted in an increase in the luciferase activity under normoxic conditions, it

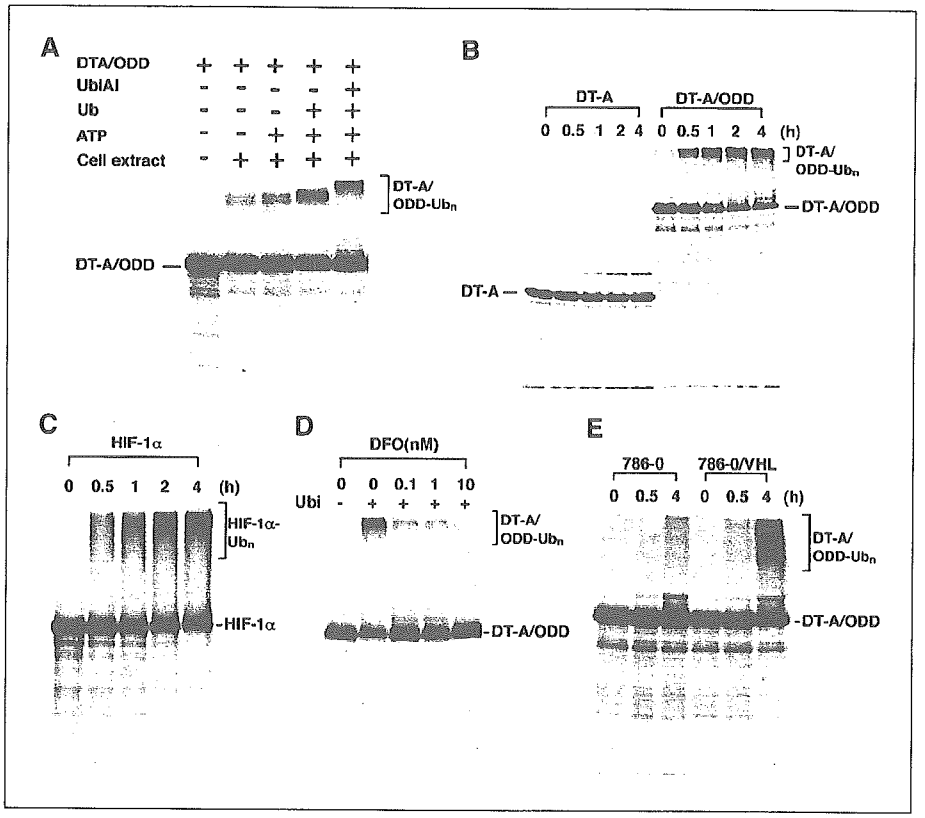

Figure 1. Oxygen- and pVHL-dependent ubiquitination of DT-A/ODD. *A, in vitro* ubiquitination of DT-A/ODD. ^{35}S-labeled DT-A/ODD was subjected to *in vitro* ubiquitination in reactions of different composition. Additions are indicated as follows: 293T S100 fraction (*cell extract*), ATP-regenerating system (*ATP*), ubiquitin (*Ub*), and ubiquitin aldehyde (*UbAl*). The mixture was incubated for 4 hours at 30°C. *B*, time course of ubiquitination of DT-A and DT-A/ODD proteins. ^{35}S-labeled DT-A and DT-A/ODD proteins were subjected to *in vitro* ubiquitination in reactions containing all components described above. *C*, ubiquitination of HIF-1α. ^{35}S-labeled HIF-1α was subjected to *in vitro* ubiquitination assay as in (*B*) for the indicated period. *D*, oxygen-dependent ubiquitination of DT-A/ODD. ^{35}S-labeled DT-A/ODD was subjected to *in vitro* ubiquitination assay in the presence or absence of ubiquitin. The mixture was incubated for 4 hours in the presence of the indicated concentrations of desferrioxamine (*DFO*). *E*, pVHL-dependent ubiquitination of DT-A/ODD. ^{35}S-labeled DT-A/ODD was subjected to *in vitro* ubiquitination assay as in (*B*) for the indicated period, except using S100 fraction prepared from 786-O or 786-O/VHL cells.

greatly enhanced the activity under hypoxic conditions in both cells. Similar results were obtained in human mammary carcinoma MCF7 cells and human foreskin fibroblasts (data not shown). Thus, EBBS caused a marked enhancement in luciferase activity in different cell types in hypoxia probably due to its mRNA-stabilizing effect.

***In vitro* protein synthesis inhibition by diphtheria toxin A, DT-A/ODD, and its attenuated fusion proteins.** We next examined whether fusion of HIF-1α ODD domain to DT-A affects the translation inhibitory activity of DT-A. For this, we first made *in vitro* translated DT-A and DT-A/ODD and then added them to the *in vitro* luciferase gene transcription/translation system with or without exogenously added NAD^+. Figure 3 shows the amount of translated ^{35}S-labeled luciferase protein. DT-A significantly reduced the level of luciferase protein even in the absence of exogenous NAD^+ and nearly completely inhibited the translation in the presence of NAD^+. DT-A/ODD was comparable with DT-A in inhibiting translation. We also made attenuated DT-A/ODD proteins, DT-A^{W153F}/ODD and DT-A^{H21A}/ODD, and measured their translation inhibitory activities in a similar way. DT-A^{W153F} and DT-A^{H21A} have been reported to have about a 4-fold and 120-fold reduced ADP ribosyltransferase activity compared with DT-A, respectively (40, 41). Consistent with the reports, DT-A^{W153F}/ODD was less effective in inhibiting the synthesis of luciferase protein compared with DT-A/ODD. DT-A^{H21A}/ODD exhibited the least inhibitory activity.

Induction of apoptosis by DT-A/ODD proteins in A11 cells under hypoxic conditions. Based on the above results, we constructed DT-A expression plasmids, pVEGFpro-DT-A/ODD-EBBS, pVEGFpro-DT-A^{W153F}/ODD-EBBS, and pVEGFpro-DT-A^{H21A}/ODD-EBBS. To investigate the effect of these expression plasmids on apoptosis of A11 cells under normoxic and hypoxic conditions, we transfected each of them into A11 cells, cultured the cells under normoxic or hypoxic conditions for 24 hours, and then stained them for Annexin V. The transfection efficiency was 20% to 30% as assessed by pEGFP-N1 expression vector. As shown in Fig. 4*A*, hypoxia alone did not induce apoptosis in the control

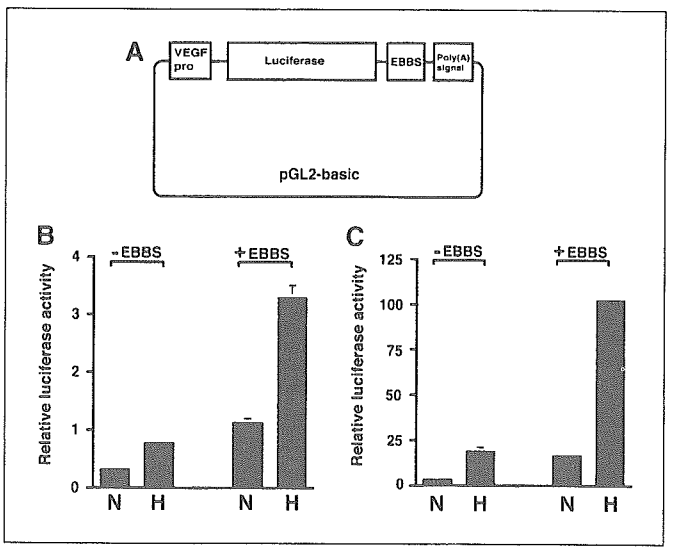

Figure 2. Effect of EBBS on the expression level of a heterologous gene under hypoxic conditions. *A*, schematic representation of the luciferase reporter constructs. *VEGFpro*, VEGF gene promoter. *B* and *C*, effect of EBBS on the expression level of a luciferase reporter gene. A11 or HepG2 cells cotransfected with pVEGFpro-Luc or pVEGFpro-Luc-EBBS and pRL-CMV as an internal control were cultured for 18 hours under normoxic (*N*) or hypoxic (*H*) conditions. All luciferase activities were normalized for transfection efficiency and background luciferase activities obtained from cells transfected with a promoterless luciferase gene *pGL2-basic* were subtracted from this value. *Columns*, luciferase activity expressed in arbitrary units; *bars*, SD of triplicate determinations.

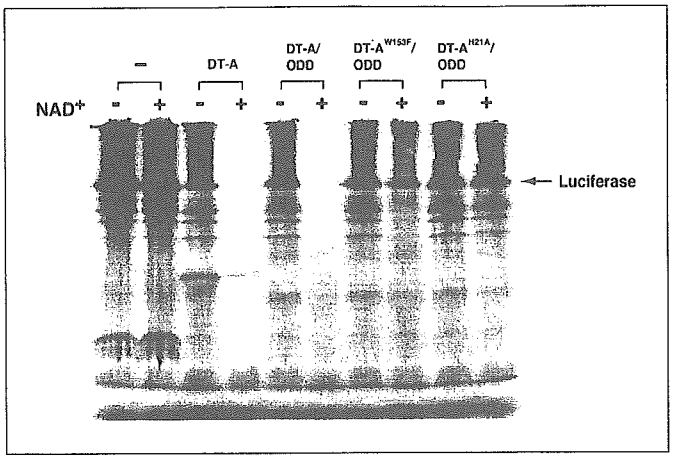

Figure 3. *In vitro* protein synthesis inhibitory activity of wild-type and attenuated DT-A/ODD fusion protein. DT-A/ODD, DT-A^{W153F}/ODD, or DT-A^{H21A}/ODD prepared by TNT T7 Quick Coupled Transcription/Translation System was added to TNT SP6 Quick Coupled Transcription/Translation mixture composed of [^{35}S]PRO-MIX and luciferase SP6 control DNA. The reaction mixtures were incubated for 90 minutes at 30°C in the presence or absence of NAD$^+$. Newly synthesized luciferase protein was separated on SDS-PAGE and detected by autoradiography.

plasmid-transfected cells, thus excluding nonspecific induction of apoptosis. The reason why ~ 10% of Annexin V–positive cells were observed in the control plasmid-transfected cells is unknown; however, it may be due to the toxicity of the transfection reagent. Expression of DT-A/ODD proteins resulted in a significant increase in the number of Annexin V–positive cells irrespective of oxygen tension. Expression of DT-A^{W153F}/ODD or DT-A^{H21A}/ODD did not apparently induce apoptosis under normoxic conditions. In contrast, they significantly caused an increase in the number of Annexin V–positive cells under hypoxic conditions, DT-A^{W153F}/ODD being more potent than DT-A^{H21A}/ODD (Fig. 4*A* and *B*). Similar results were obtained in their abilities to induce sub-G_1 fraction, another criteria of apoptosis, under hypoxic conditions (Fig. 4*C*). Long-term exposure of A11 cells to severe hypoxia resulted in cell death to some extent, but expression of DT-A^{W153F}/ODD further enhanced cell death (Fig. 4*D*). Thus, transfection of pVEGFpro-DT-A^{W153F}/ODD-EBBS or pVEGFpro-DT-A^{H21A}/ODD-EBBS plasmid into A11 cells led to a clear hypoxia-dependent induction of apoptosis.

Establishment of A11H10 cells with higher resistance to hypoxia-induced apoptosis. We next wanted to investigate the effect of liposomal gene transfer of the DT-A/ODD expression construct on induction of apoptosis in hypoxic regions of tumors. Before this experiment, we established A11H10 cells with higher resistance to hypoxia-induced apoptosis than A11 cells and used them as target cells. The cells were actually more resistant to apoptosis induced by severe hypoxia (<0.1% O_2) than A11 cells (Fig. 5*A*) and survived for >5 days in severe hypoxia (Fig. 5*B*). They were also more resistant to apoptosis triggered by an anticancer drug cisplatin than A11 cells (Fig. 5*C*). The apoptosis-resistant phenotype was stable at least for 3 months (data not shown). A11H10 cells expressed VEGF mRNA as well as A11 cells in response to hypoxia (Fig. 5*D*).

Apoptosis induction by liposomal transfer of diphtheria toxin A expression plasmid in hypoxic regions of A11H10 tumors. From the results described above, we chose the pVEGFpro-DT-A^{W153F}/ODD-EBBS expression construct and examined its effect on apoptosis induction in tumors. Before this experiment, we directly injected pEGFP-N1/DIMRIE-C complex in A11H10 tumors along with lysine-fixable dextran-TMR to see if we can use dextran-TMR for later identification of injected areas. Two days after the injection, tumors were surgically removed and cryosections were prepared. Observation of the specimen revealed that EGFP-expressing tumor cells located in dextran-TMR–positive areas, indicating that dextran-TMR can be used to identify injected areas (Fig. 6). We then intratumorally injected pVEGFpro or pVEGFpro-DT-A^{W153F}/ODD-EBBS/DMRIE-C complex together with

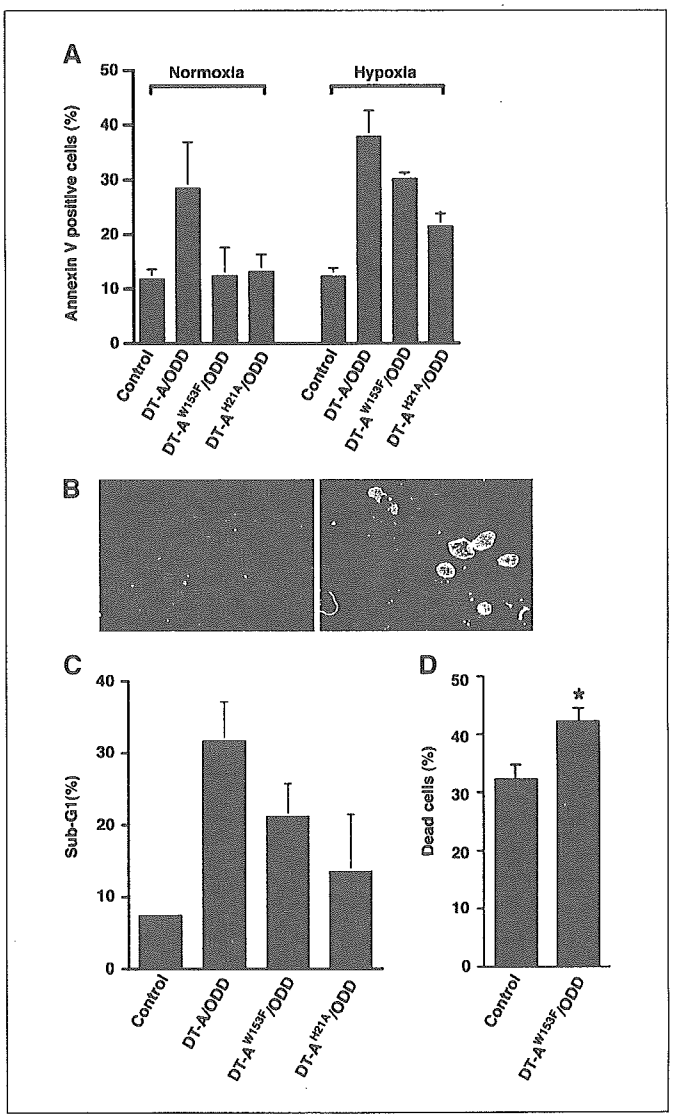

Figure 4. Induction of apoptosis in A11 cells transfected with pVEGFpro-DT-A/ODD-EBBS, pVEGFpro-DT-A^{W153F}/ODD-EBBS, and pVEGFpro-DT-A^{H21A}/ODD-EBBS vectors. A11 cells were transiently transfected with pVEGFpro as a control, pVEGFpro-DT-A/ODD-EBBS, pVEGFpro-DT-A^{W153F}/ODD-EBBS, and pVEGFpro-DT-A^{H21A}/ODD-EBBS. After culturing the cells under normoxic or hypoxic conditions for 24, 36, or 48 hours, the cells were processed for Annexin V staining (*A* and *B*), sub-G_1 analysis (*C*), or trypan blue dye exclusion test (*D*), respectively. *A*, induction of Annexin V–positive cells by the expression vectors. *B*, Annexin V–positive cells induced by the transfection of pVEGFpro-DT-A^{W153F}/ODD-EBBS in normoxia (*left*) or hypoxia (*right*). The fluorescence was observed under a confocal laser microscope. *C*, induction of cellular DNA fragmentation (sub-G_1) by the expression vectors in hypoxia. *Columns*, percentage of sub-G_1 fraction determined with a FACScan flow cytometer. *D*, induction of cell death by the expression vectors in severe hypoxia. *Columns*, percentage of dead cells; *bars*, SD of triplicate determinations. *, $P < 0.007$.

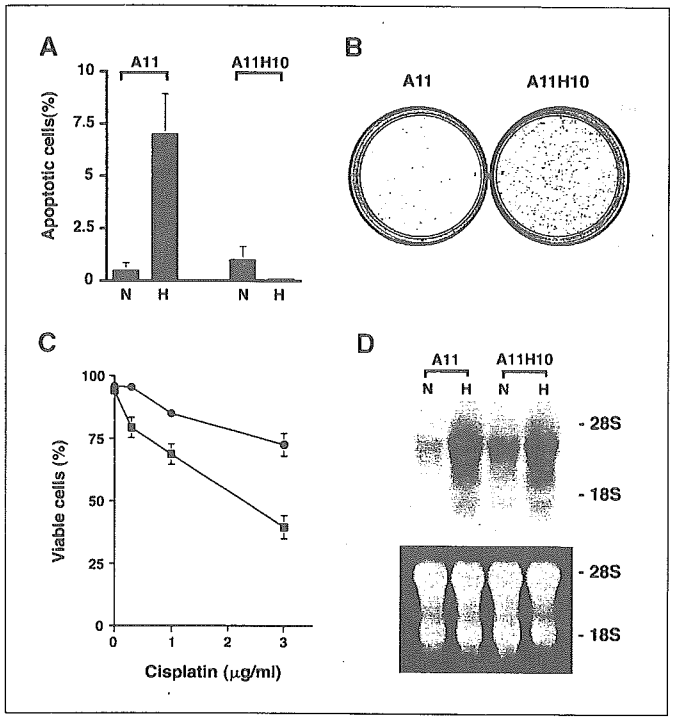

Figure 5. Establishment and characterization of A11H10 cells. *A*, apoptosis of A11 and A11H10 cells in severe hypoxia. The cells were cultured in normoxia or severe hypoxia (<0.1% O_2; *H*) for 28 hours and the percentage of cells with chromatin condensation and fragmentation was determined after DAPI staining. *Columns*, percentage of apoptotic cells; *bars*, SD of triplicate determinations. *B*, survival of A11 and A11H10 cells in severe hypoxia. The cells (1×10^5) were cultured in severe hypoxia (<0.1% O_2) for 5 days followed by culturing in normoxia for 7 days. Colonies were stained with crystal violet. *C*, sensitivity of A11 and A11H10 cells to cisplatin. The cells were exposed to the indicated concentrations of cisplatin for 2 days. Cell viability was assessed by trypan blue dye exclusion. *Points*, percentage of viable cells; *bars*, SD of triplicate determinations. *D*, *VEGF* mRNA expression in A11 and A11H10 cells. Total RNA was isolated from the cells cultured in normoxia or hypoxia for 8 hours and subjected to Northern analysis. Blots were hybridized with ^{32}P-labeled mouse *VEGF* cDNA. Ethidium bromide staining of the gel is also shown.

dextran-TMR, and 2 days after the injection we administered EF5 for discrimination between normoxic and hypoxic regions. Cryosections were prepared and processed for TUNEL staining followed by staining with Cy5-labeled anti-EF5 antibody and Hoechst staining. We omitted necrotic areas from the analyses. The results showed that a few TUNEL-positive cells were observed in dextran-TMR–negative areas of both control and pVEGFpro-DT-A^{W153F}/ODD-EBBS plasmid-injected tumors (Fig. 7*A* and *C*), whereas a large number of TUNEL-positive cells were detected in dextran-TMR-positive areas of the pVEGFpro-DT-A^{W153F}/ODD-EBBS-injected tumors (Fig. 7*D*) but not of the pVEGFpro-injected tumors (Fig. 7*B*). Closer observations of the specimen of the pVEGFpro-DT-A^{W153F}/ODD-EBBS-injected tumors revealed that only a small number of TUNEL-positive cells were evident in dextran-TMR–positive and EF5-negative (normoxic) areas (Fig. 8*A-D*), whereas a large number of TUNEL-positive cells were detected in dextran-TMR-positive and EF5-positive (hypoxic) areas (Fig. 8*E-H*). Thus, these results indicate that apoptosis was remarkably induced by liposomal transfer of pVEGF-DT-A^{W153F}/ODD-EBBS expression construct in hypoxic, but not in normoxic, regions of A11H10 tumors.

Tumor growth inhibition by liposomal transfer of diphtheria toxin A expression plasmi d in P29 tumors. Based on the

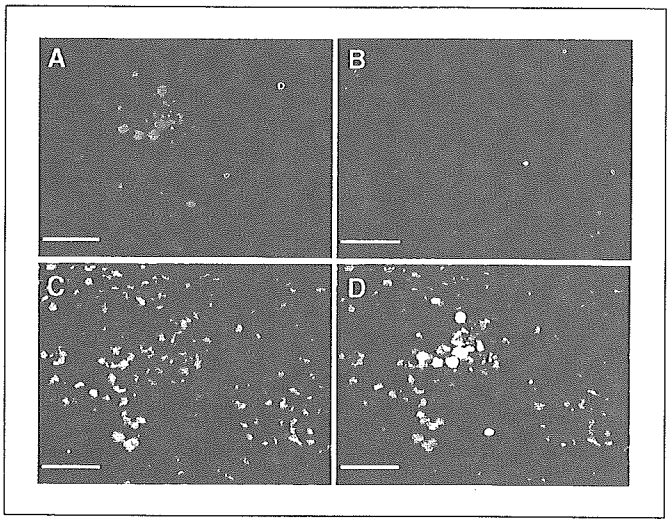

Figure 6. Liposomal gene transfer of pEGFP-N1 into A11H10 tumors. pEGFP-N1/DMRIE-C complex was directly injected into s.c. A11H10 tumors along with dextran-TMR. Two days after the injection, cryosections were prepared, stained with Hoechst 33342, and then observed under a fluorescent microscope for EGFP (*green*), dextran-TMR (*orange*), and Hoechst 33342 (*blue*). Images were captured using a Cool SNAP charge-coupled device camera and pseudocolored by a RS IMAGE Express image processing software. *A*, EGFP. *B*, dextran-TMR. *C*, Hoechst33342. *D*, merged. Note that EGFP-expressing cells locate in dextran-TMR-positive areas. Bar, 50 μm.

above results, we repeatedly injected pVEGF-DT-A^{W153F}/ODD-EBBS/liposome complex into A11H10 tumors to see the therapeutic effect of the plasmid. However, the inhibition of tumor growth was marginal (data not shown). We speculated that this is due to the fact that A11 tumors are well vascularized (42) and, hence, not so hypoxic. We then used P29 tumors because they are poorly vascularized (42). Actually, as expected, EF5 staining showed that P29 tumors contained increased hypoxic areas compared with A11H10 tumors (Fig. 9*A* and *B*). We therefore examined the effect

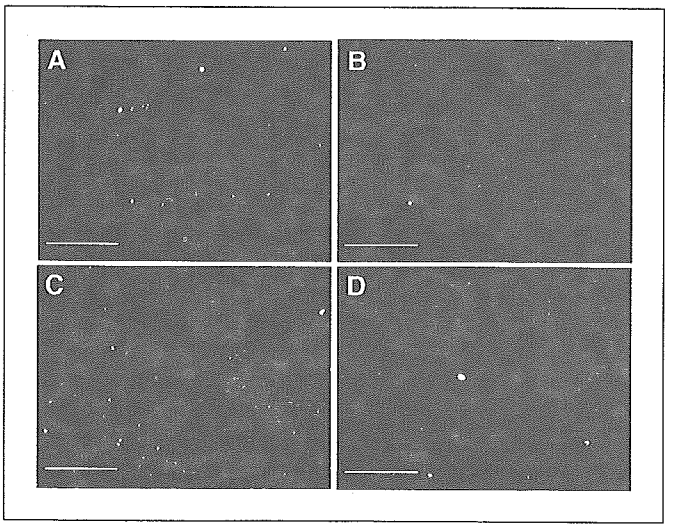

Figure 7. Apoptosis induction by liposomal gene transfer of pVEGFpro-DT-A^{W153F}/ODD-EBBS into A11H10 tumors. pVEGFpro as a control (*A* and *B*) or pVEGFpro-DT-A^{W153F}/ODD-EBBS/DMRIE-C complex (*C* and *D*) was directly injected into A11H10 tumors along with dextran-TMR. Two days after the injection, cryosections were prepared, stained for TUNEL, and observed under a confocal microscope for TUNEL-positive cells (*green*) and dextran-TMR (*orange*). *A* and *C*, dextran-TMR–positive areas. *B* and *D*, dextran-TMR–negative areas. Bar, 100 μm.

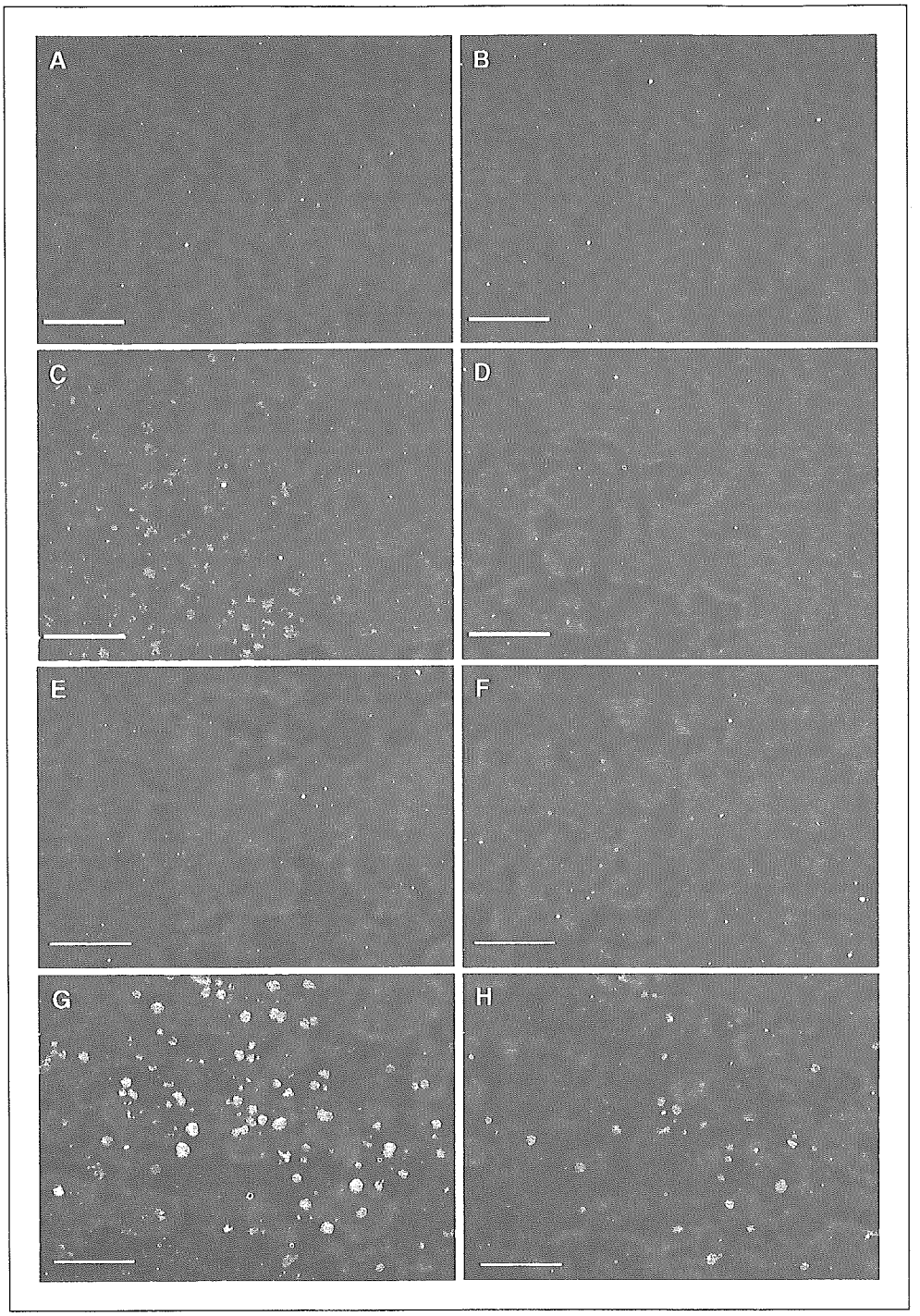

Figure 8. Apoptosis induction in hypoxic areas of A11H10 tumors after liposomal gene transfer of pVEGFpro-DT-A^{W153F}/ODD-EBBS. pVEGFpro-DT-A^{W153F}/ODD-EBBS/DMRIE-C complex was directly injected into A11H10 tumors along with dextran-TMR. Two days after the injection, the mice were administered with EF5. The cryosections of tumors were successively processed for TUNEL, EF5, and Hoechst 33342 stainings. Images were captured using a Cool SNAP charge-coupled device camera and pseudocolored by a RS IMAGE Express image processing software. TUNEL (*green*), EF5 (*pink*), Hoechst 33342 (*blue*), and dextran-TMR (*orange*). *A* to *D*, dextran-TMR–positive and EF5-negative areas. *E* to *H*, dextran-TMR–positive and EF5-positive areas. *A* and *E*, dextran-TMR. *B* and *F*, EF5. *C* and *G*, merged image of TUNEL and Hoechst 33342. *D* and *H*, merged image of TUNEL, EF5, and dextran-TMR. Bar, 50 μm.

of multiple injections of the expression construct on P29 tumor growth. The results showed that a modest but statistically significant growth inhibition was observed in the mice with pVEGF-DT-A^{W153F}/ODD-EBBS compared with the mice with pVEGFpro without apparent side effects, such as body weight loss (Fig. 10*A* and *B*).

Discussion

In this study, we examined the effectiveness of VEGF promoter–driven DT-A expression for killing hypoxic tumor cells. To reduce cytotoxicity of DT-A in normal cells and increase hypoxia specificity, we constructed the expression vector to express DT-A/ODD fusion protein to produce mRNA containing the EBBS and not to include unnecessary enhancer/promoter sequence other than VEGF promoter. The results showed that DT-A/ODD, but not DT-A, was ubiquitinated as well as HIF-1α in a pVHL- and oxygen-dependent manner in *in vitro* ubiquitination assays. The EBBS exhibited mRNA-stabilizing effect, as shown by luciferase reporter assays. Thus, HIF-1α ODD domain and the EBBS worked accordingly. In addition, DT-A/ODD exhibited a comparable inhibitory activity of protein synthesis with DT-A *in vitro*, indicating that fusion of the ODD domain to DT-A does not affect its translation inhibitory activity.

The ODD domain of HIF-1α has been implicated to be useful as a hypoxia switch, limiting the production of a fusion protein in normoxia while stabilizing it in hypoxia (43). For example, ODD–caspase-3 fusion protein is shown to be specifically stabilized and activated in hypoxic cells (44). The present study also showed that the ODD domain is capable of regulating the toxicity of attenuated DT-A, probably rendering the fusion protein to be recognized by pVHL and subsequently degraded through proteasome pathway. However, we presently have no evidence that these events actually occur in the cells.

ERBP was initially identified as the protein(s) that specifically binds to a 120 base fragment (EBBS) of the 3′ UTR of *Epo* mRNA. ERBP binds to this sequence and prolongs the half-life of *Epo* mRNA as well as other reporter mRNA containing EBBS in normoxia and further in hypoxia (23). Although Epo is mainly expressed in cells derived from the liver and the kidney, ERBP is present in other tissues, such as lung, brain, and spleen (23). We could also observe the reporter mRNA-stabilizing effect of EBBS in lung carcinoma cells, hepatoma cells, breast carcinoma cells, and fibroblasts. Therefore, EBBS is able to stabilize a heterologous transcript in a variety of cell types. An alternative to stabilize mRNA in hypoxia may be the use of HuR-binding sequence or recently identified PAIP2-binding sequence, both of which are present in *VEGF* mRNA (22, 45). These elements could substitute for the EBBS in the present expression vector.

Transfection of pVEGFpro-DT-A/ODD-EBBS expression vector into high-metastatic A11 cells resulted in a marked induction of apoptosis in both normoxia and hypoxia. This indicated that only a background expression level of DT-A/ODD is too cytotoxic to be regulated. We then sought to use attenuated DT-A/ODD, DT-A^{W153F}/ODD, and DT-A^{H21A}/ODD, expecting that although they are less active in inhibiting protein synthesis than DT-A/ODD under normoxic conditions, they may exhibit a significantly higher activity when expressed and accumulated in the cells under hypoxic conditions. The results showed that DT-A^{W153F}/ODD and DT-A^{H21A}/ODD were very weak in inducing apoptosis under normoxic conditions, whereas they significantly induced apoptosis under hypoxic conditions. Thus, we could observe hypoxia-dependent induction of apoptosis in A11 cells transfected with the attenuated DT-A/ODD expression vector. The pVEGFpro-DT-A^{W153F}/ODD-EBBS was superior to pVEGFpro-DT-A^{H21A}/ODD-EBBS in inducing apoptosis.

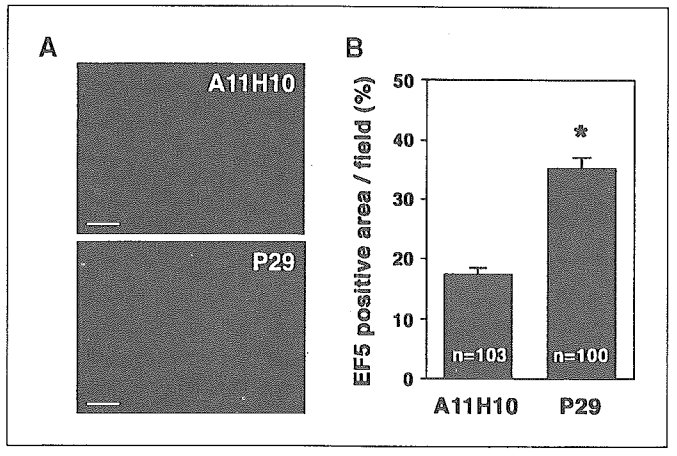

Figure 9. The degree of intratumoral hypoxia in A11H10 and P29 tumors. *A*, detection of hypoxic areas in tumors by EF5 staining. Frozen sections of s.c. tumor established from A11H10 and P29 cells were stained for EF5. Bar, 100 μm. *B*, the degree of hypoxia in A11H10 and P29 tumors. Frozen sections prepared from different regions of A11H10 and P29 tumor were stained for EF5. The fluorescent images of >100 fields (1.175 mm^2/field) were analyzed and the percentage of EF5-positive area per field (*columns*) was calculated. *Bars*, SE. *, $P < 0.0001$.

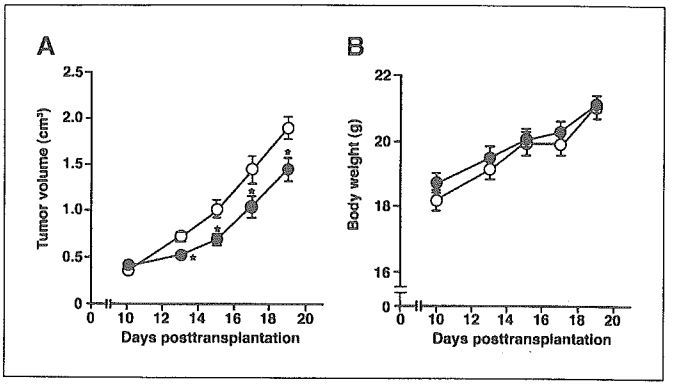

Figure 10. Growth inhibition of P29 tumors by liposomal gene transfer of pVEGFpro-DT-A^{W153F}/ODD-EBBS. *A*, growth of tumors injected with pVEGFpro (○) or pVEGFpro-DT-A^{W153F}/ODD-EBBS/DMRIE-C complex (●). The liposome complex was directly injected into the tumor daily. *B*, body weight of the mice with pVEGFpro (○) or pVEGFpro-DT-A^{W153F}/ODD-EBBS (●). *Bars*, SE. *, $P < 0.04$.

Given that the pVEGFpro-DT-A^{W153F}/ODD-EBBS vector strongly induce apoptosis in the transfected cells under hypoxic but not normoxic conditions, we decided to apply pVEGFpro-DT-A^{W153F}/ODD-EBBS vector to *in vivo* experiments. Before investigating the effect, we established A11H10 cells that are highly resistant to hypoxia-induced apoptosis. We previously reported that A11 cells are more resistant to apoptosis induced by microenvironmental stresses than low-metastatic counterparts (8). A11H10 cells were further more resistant than A11 cells to not only hypoxia but also anticancer drugs and various ER stresses (glucose deprivation, tunicamycin, brefeldin A, calcium ionophore A23187; data not shown). Therefore, the cells enabled us to examine the effect of the expression vector on the tumors that are more difficult to cure. After establishing s.c. A11H10 tumors, we directly injected pVEGFpro-EBBS/liposome complex as a control or pVEGFpro-DT-A^{W153F}/ODD-EBBS/liposome complex with dextran-TMR conjugates, which are frequently used for long-term tracers of live cells. Dextran-TMR conjugates were not toxic and could be detected in the tumors at least 3 days after the injection (data not shown) and, therefore, it was useful to monitor the injection areas of DNA/liposome complex. Actually, EGFP was expressed in cells located in dextran-TMR–positive areas in the tumors administrated with pEGFP-N1 plasmid/DMRIE-C complex. To detect hypoxic areas in the tumors, we used EF5, a derivative of nitroimidazole (39). The results showed that pVEGFpro-EBBS/liposome administration hardly induced apoptotic (TUNEL-positive) cells in dextran-TMR–positive areas. In contrast, pVEGFpro-DT-A^{W153F}/ODD-EBBS/liposome administration resulted in a striking induction of apoptosis in dextran-TMR–positive areas. More specifically, apoptotic cells were detected in hypoxic, but not in normoxic, areas of pVEGFpro-DT-A^{W153F}/ODD-EBBS/liposome-administered tumors. These results clearly indicate that intratumoral injection of pVEGFpro-DT-A^{W153F}/ODD-EBBS/liposome complex induced apoptosis in a hypoxia-dependent fashion. It should be noted, however, that we could not observe a clear tumor growth inhibition after multiple injection of pVEGFpro-DT-A^{W153F}/ODD-EBBS/liposome complex into a tumor mass. This contrasts to the case of direct injection of α-fetoprotein promoter/

enhancer-driven DT-A expression construct/DMRIE-C complex into hepatoma in which significant growth retardation was observed (33). However, our results rather seem to reflect the hypoxia specificity of our expression construct. Because total hypoxic areas in an A11H10 tumor mass are small relative to total normoxic areas, an obvious growth inhibition may not be observed even if all hypoxic tumor cells are killed. Then, to test the therapeutic effect of the expression vector in more hypoxic tumors, we chose P29 tumors that have poorer vasculature and, thus, are more hypoxic than A11 tumors. As a result, we could clearly observe growth retardation of the tumor. Although the effect was not so striking, it may be due to the hypoxia specificity and inefficient *in vivo* gene transfer.

The present DT-A^{W153F}/ODD expression vector would be applicable to a wide variety of tumors, especially those with severe hypoxia, such as cervical cancer and melanomas (46). These cancers are also suitable for intratumoral gene delivery. A critical point to be improved in the future is the transfection method of the vector into hypoxic tumor cells. Although liposomes used here have many advantages as a gene transfer method, such as low evocation of inflammations and immune responses, transfection efficiency is not so high. A solution to this point may be the use of adenoviruses and recently developed DT-resistant packaging line (34), which may allow us to produce a high titer of adenoviruses encoding DT-A^{W153F}/ODD. Combination of such adenoviruses and conventional therapeutic regimens may lead to total killing of tumor cells and ultimately prevention of tumor recurrence.

Acknowledgments

Received 1/13/2005; revised 8/24/2005; accepted 9/30/2005.

Grant support: Grant-in-aid from the Ministry of Health, Labour, and Welfare for Third Term Comprehensive Control Research for Cancer.

The costs of publication of this article were defrayed in part by the payment of page charges. This article must therefore be hereby marked *advertisement* in accordance with 18 U.S.C. Section 1734 solely to indicate this fact.

We thank Dr. S. Fujimoto for his support.

References

1. Brown JM, Giaccia AJ. The unique physiology of solid tumors: opportunities (and problems) for cancer therapy. Cancer Res 1998;58:1408–16.
2. Chaplin DJ, Hill SA. Temporal heterogeneity in microregional erythrocyte flux in experimental solid tumours. Br J Cancer 1995;71:1210–3.
3. Teicher BA. Hypoxia and drug resistance. Cancer Metastasis Rev 1994;13:139–68.
4. Cairns RA, Kalliomaki T, Hill RP. Acute (cyclic) hypoxia enhances spontaneous metastasis of KHT murine tumors. Cancer Res 2001;61:8903–8.
5. Pennacchietti S, Michieli P, Galluzzo M, et al. Hypoxia promotes invasive growth by transcriptional activation of the met protooncogene. Cancer Cell 2003;3:347–61.
6. Staller P, Sulitkova J, Lisztwan J, et al. Chemokine receptor CXCR4 downregulated by von Hippel-Lindau tumour suppressor pVHL. Nature 2003;425:307–11.
7. Graeber TG, Osmanian C, Jacks T, et al. Hypoxia-mediated selection of cells with diminished apoptotic potential in solid tumours. Nature 1996;379:88–91.
8. Takasu M, Tada Y, Wang JO, Tagawa M, Takenaga K. Resistance to apoptosis induced by microenvironmental stresses is correlated with metastatic potential in Lewis lung carcinoma. Clin Exp Metastasis 1999;17:409–16.
9. Rice GC, Hoy C, Schimke RT. Transient hypoxia enhances the frequency of dihydrofolate reductase gene amplification in Chinese hamster ovary cells. Proc Natl Acad Sci U S A 1986;83:5978–82.
10. Russo CA, Weber TK, Volpe CM, et al. An anoxia inducible endonuclease and enhanced DNA breakage as contributors to genomic instability in cancer. Cancer Res 1995;55:1122–8.
11. Coquelle A, Toledo F, Stern S, Bieth A, Debatisse M. A new role for hypoxia in tumor progression: induction of fragile site triggering genomic rearrangements and formation of complex DMs and HSRs. Mol Cell 1998;2:259–65.
12. Goldberg MA, Schneider TJ. Similarities between the oxygen-sensing mechanisms regulating the expression of vascular endothelial growth factor and erythropoietin. J Biol Chem 1994;269:4355–9.
13. Goldberg MA, Glass GA, Cunningham JM, Bunn HF. The regulated expression of erythropoietin by two human hepatoma cell lines. Proc Natl Acad Sci U S A 1987;84:7972–6.
14. Ikeda E, Achen MG, Breier G, Risau W. Hypoxia-induced transcriptional activation and increased mRNA stability of vascular endothelial growth factor in C6 glioma cells. J Biol Chem 1995;270:19761–6.
15. Wenger RH, Gassmann M. Oxygen(s) and the hypoxia-inducible factor-1. Biol Chem 1997;378:609–16.
16. Hofer T, Wenger H, Gassmann M. Oxygen sensing, HIF-1α stabilization and potential therapeutic strategies. Pflugers Arch 2002;443:503–7.
17. Forsythe JA, Jiang BH, Iyer NV, et al. Activation of vascular endothelial growth factor gene transcription by hypoxia-inducible factor 1. Mol Cell Biol 1996;16:4604–13.
18. Maxwell PH, Wiesener MS, Chang GW. et al. The tumour suppressor protein VHL targets hypoxia-inducible factors for oxygen-dependent proteolysis. Nature 1999;399:271–5.
19. Ivan M, Kaelin WG, Jr. The von Hippel-Lindau tumor suppressor protein. Curr Opin Genet Dev 2001;11:27–34.
20. Jaakkola P, Mole DR, Tian YM, et al. Targeting of HIF-α to the von Hippel-Lindau ubiquitylation complex by O_2-regulated prolyl hydroxylation. Science 2001;292:468–72.
21. Jewell UR, Kvietikova I, Scheid A, et al. Induction of HIF-1α in response to hypoxia is instantaneous. FASEB J 2001;15:1312–4.
22. Goldberg-Cohen I, Furneauxb H, Levy AP. A 40-bp RNA element that mediates stabilization of vascular endothelial growth factor mRNA by HuR. J Biol Chem 2002;277:13635–40.
23. McGary EC, Rondon IJ, Beckman BS. Post-transcriptional regulation of erythropoietin mRNA stability by erythropoietin mRNA-binding protein. J Biol Chem 1997;272:8628–34.
24. Dachs GU, Patterson AV, Firth JD, et al. Targeting gene expression to hypoxic tumor cells. Nat Med 1997;3:515–20.
25. Koshikawa N, Takenaga K, Tagawa M, Sakiyama S. Therapeutic efficacy of the suicide gene driven by the promoter of vascular endothelial growth factor gene against hypoxic tumor cells. Cancer Res 2000;60:2936–41.
26. Harris AL. Hypoxia—a key regulatory factor in tumour growth. Nat Rev Cancer 2002;2:38–47.
27. Binley K, Askham Z, Martin L, et al. Hypoxia-mediated tumour targeting. Gene Ther 2003;10:540–9.
28. Collier RJ. Diphtheria toxin: mode of action and structure. Bacteriol Rev 1975;39:54–85.
29. Vingerhoeds MH, Steerenberg PA, Hendriks JJ, et al. Targeted delivery of diphtheria toxin via immunoliposomes: efficient antitumor activity in the presence of inactivating anti-diphtheria toxin antibodies. FEBS Lett 1996;395:245–50.
30. Kreitman RJ. Immunotoxins in cancer therapy. Curr Opin Immunol 1999;11:570–8.
31. Maxwell IH, Maxwell F, Glode LM. Regulated expression of a diphtheria toxin A-chain gene transfected into human cells: possible strategy for inducing cancer cell suicide. Cancer Res 1986;46:4660–4.
32. Hall PD, Willingham MC, Kreitman RJ, Frankel AE. DT388-GM-CSF, a novel fusion toxin consisting of a truncated diphtheria toxin fused to human granulocyte-macrophage colony-stimulating factor, prolongs host survival in a SCID mouse model of acute myeloid leukemia. Leukemia 1999;13:629–33.
33. Kunitomi M, Takayama E, Suzuki S, et al. Selective inhibition of hepatoma cells using diphtheria toxin A under the control of the promoter/enhancer region of the human α-fetoprotein gene. Jpn J Cancer Res 2000;91:343–50.
34. Li Y, McCadden J, Ferrer F, et al. Prostate-specific expression of the diphtheria toxin A chain (DT-A): studies of inducibility and specificity of expression of prostate-specific antigen promoter-driven DT-A adenoviral-mediated gene transfer. Cancer Res 2002;62:2576–82.
35. Keyvani K, Baur I, Paulus W. Tetracyclin-controlled expression but not toxicity of an attenuated diphtheria toxin mutant. Life Sci 1999;64:1719–24.
36. Kimura H, Weisz A, Kurashima Y, et al. Hypoxia response element of the human vascular endothelial growth factor gene mediates transcriptional regulation by nitric oxide: control of hypoxia-inducible factor-1 activity by nitric oxide. Blood 2000;95:189–97.
37. Cockman ME, Masson N, Mole DR, et al. Hypoxia inducible factor-α binding and ubiquitylation by the von Hippel-Lindau tumor suppressor protein. J Biol Chem 2000;275:25733–41.
38. Epinat J-C, Gilmore TD. *In vitro*-translated diphtheria toxin A chain inhibits translation in wheat germ extracts: analysis of biologically active, caspase-3-resistant diphtheria toxin mutants. Biochim Biophys Acta 1999;1472:34–41.
39. Lord EM, Harwell L, Koch CJ. Detection of hypoxic cells by monoclonal antibody recognizing 2-nitroimidazole adducts. Cancer Res 1993;53:5721–6.
40. Zdanovskaia MV, Zdanovsky AG, Yankovsky NK. Diphtheria toxin NAD affinity and ADP ribosyltransferase activity are reduced at tryptophan 153 substitutions for alanine or phenylalanine. Res Microbiol 2000;151:557–62.
41. Blanke SR, Huang K, Wilson BA, et al. Active-site mutations of the diphtheria toxin catalytic domain: role of histidine-21 in nicotinamide adenine dinucleotide binding and ADP-ribosylation of elongation factor 2. Biochemistry 1994;33:5155–61.
42. Koshikawa N, Iyozumi A, Gassmann M, Takenaga K. Constitutive upregulation of hypoxia-inducible factor-1α mRNA occurring in highly metastatic lung carcinoma cells leads to vascular endothelial growth factor overexpression upon hypoxic exposure. Oncogene 2003;22:6717–24.
43. Payen E, Bettan M, Henri A, et al. Oxygen tension and a pharmacological switch in the regulation of transgene expression for gene therapy. J Gene Med 2001;3:498–504.
44. Harada H, Hiraoka M, Kizaka-Kondoh S. Antitumor effect of TAT-oxygen-dependent degradation-caspase-3 fusion protein specifically stabilized and activated in hypoxic tumor cells. Cancer Res 2002;62:2013–8.
45. Onesto C, Berra E, Grepin R, Pages G. Poly(A) binding protein-interacting protein 2, a strong regulator of vascular endothelial growth factor mRNA. J Biol Chem 2004;279:34217–26.
46. Dachs GU, Tozer GM. Hypoxia-modulated gene expression: angiogenesis, metastasis and therapeutic exploitation. Eur J Cancer 2000;36:1649–60.

Journal of Neuroscience Research 83:619–626 (2006)

Sensory Neurite Outgrowth on White Matter Astrocytes Is Influenced by Intracellular and Extracellular S100A4 Protein

Z. Fang,[1] N. Forslund,[1] K. Takenaga,[1,2] E. Lukanidin,[3] and E.N. Kozlova[1]*

[1]Department of Neuroscience, Biomedical Center, Uppsala University, Uppsala, Sweden
[2]Division of Chemotherapy, Chiba Cancer Center Research Institute, Chiba, Japan
[3]Laboratory of Cancer Molecular Biology, Danish Cancer Society, Copenhagen, Denmark

The central nervous system (CNS) is considered a nonpermissive environment for axonal regeneration because of the presence of myelin and associated repulsive molecules. However, neural cells transplanted to the CNS preferably migrate and extend their fibers in white matter areas. We previously showed that white matter astrocytes in vivo express the calcium-binding protein S100A4, which is strongly up-regulated in areas of white matter degeneration. To investigate the role of white matter astrocytes and their specific protein S100A4 in axonal regeneration, we developed white matter astrocyte cultures with strong S100A4 expression and grew dissociated adult dorsal root ganglion (DRG) cells on top of astrocytes for 24 hr. By using small interfering S100A4 RNA, we were able to eliminate S100A4 expression and compare growth of DRG cell neurites on S100A4-silenced and S100A4-expressing astrocytes. In addition, we studied whether extracellular S100A4 has an effect on neurite growth from adult DRG cells cultured on S100A4-expressing white matter astrocytes. Our data show that white matter astrocytes are permissive for neurite growth, although high levels of S100A4 in white matter astrocytes have a negative effect on this growth. Extracellular application of S100A4 induced extensive growth of DRG cell neurites on white matter astrocytes. These findings suggest that white matter astrocytes are able to support axonal regeneration and, furthermore, that administration of extracellular S100A4 provides strong additional support for axonal regeneration.

Key words: nerve regeneration; dorsal root ganglion; calcium-binding protein; siRNA; in vitro

Central nervous system (CNS) white matter is considered nonpermissive for axonal regeneration. This attribute is the result mainly of observations that myelin-associated molecules cause growth cone collapse in vitro and inhibit axonal elongation in vivo (for review see Spencer et al., 2003). However, dorsal root ganglion (DRG) cells, which are microtransplanted into normal or degenerating CNS white matter, readily extend axons for long distances, indicating that white matter is, indeed, able to support axonal regeneration (Davies et al., 1997, 1999). The factors that support neurite growth in CNS white matter are incompletely known. The strong association between oligodendrocytes and neurite growth inhibition suggests that support for axon extension is provided by astrocytes, the other major cell component in CNS white matter. Recent findings indicate that astroglial-associated fibronectin is one factor that promotes DRG cell neurite outgrowth in mature CNS white matter (Tom et al., 2004).

Astrocytes in white matter selectively express S100A4 (Kozlova and Lukanidin, 1999; Åberg and Kozlova, 2000), a calcium-binding protein of the EF-hand type with multiple intra- and extracellular activities (for review see Helfman et al., 2005). The S100A4 protein is encoded by the *S100A4* gene, which was originally identified in metastatic tumor cells. S100A4 has potent tumorigenic effects, presumably mediated through several mechanisms, including modification of the cytoskeleton, dysregulation of the tumor suppressor p53, and stimulation of angiogenesis. The role of S100A4 in the CNS is unknown. However, S100A4 is markedly and exclusively up-regulated in white matter astrocytes following injury (Kozlova and Lukanidin, 1999, 2002; see also Zhang et al., 2004), suggesting a role for the protein in modifying the functional properties of astrocytes in degenerating white matter. These modifications may influ-

Contract grant sponsor: The Swedish Science Council; Contract grant number: 5420.

*Correspondence to: Elena N. Kozlova, PhD, Department of Neuroscience, Biomedical Center, P.O. Box 587, SE-751 23 Uppsala, Sweden. E-mail: elena.kozlova@anatomi.uu.se

Received 26 July 2005; Revised 7 November 2005; Accepted 8 November 2005

Published online 24 January 2006 in Wiley InterScience (www.interscience.wiley.com). DOI: 10.1002/jnr.20743

ence the possibilities for injured axons to regenerate in the CNS.

Here, we explore the role of S100A4 for neurite outgrowth from dissociated adult DRG neurons placed on cultured white matter astrocytes. Injury to the central (dorsal root) axons of DRG neurons represents a prototypic model for CNS regeneration failure in vivo. Dorsal root axons initially travel in a peripheral nervous system environment and continue into the spinal cord between processes of white matter astrocytes. Injured dorsal root axons regenerate readily in their peripheral nervous environment but cease to grow when they encounter these astrocytes. To address the specific role of S100A4 in white matter astrocytes, we applied the technique of small interfering (si) RNAs, which allows the expression of specific genes to be "silenced." By using this approach, we were able to compare the extent of neurite growth from DRG cells cultured on S100A4-expressing and -silenced white matter astrocytes.

Previous studies have shown that extracellular S100A4 is a potent stimulator of neurite outgrowth from embryonic hippocampal neurons (Novitskaya et al., 2000) and a neuroprotectant and neurite outgrowth stimulator of embryonic mesencephalic and early postnatal cerebellar neurons in vitro (Pedersen et al., 2004). However, these results were obtained in pure neuronal cultures, in the absence of neuron–astroglial interactions. Therefore, we wanted to explore whether such interactions alter the neuronal response to extracellular S100A4 in our coculture system, which more closely reflects the in vivo situation. Therefore, in addition to exploring how DRG cell neurites interact with white matter astrocytes, we have addressed the issue of how extracellular S100A4 influences DRG cell neurite outgrowth on S100A4-expressing white matter astrocytes.

Our findings show that DRG cell neurite extension is supported by S100A4-expressing as well as S100A4-silenced white matter astrocytes, with the latter being the most efficient ones. Furthermore, extracellular administration of S100A4 protein strongly supported DRG cell neurite growth on S100A4-expressing white matter astrocytes.

MATERIALS AND METHODS

Astrocyte Cultures

The animal procedures were approved by the Uppsala County regional committee for research on animals. White matter astrocytes were prepared according the protocol of percol purification of corpus callosum (CC) astrocytes from postnatal day 4 (P4) rats (Kozlova and Takenaga, 2005). Briefly, 10 rat pups from P4 were decapitated. The brain was immediately removed and placed in a Petri dish with cold phosphate-buffered saline (PBS). A 4-mm-thick coronal slice at the level of hippocampus was made and placed in a Petri dish with Dulbecco's modified Eagle's medium (DMEM) containing 10% fetal calf serum (FCS) supplemented with 100 U/ml penicillin and 100 μg/ml streptomycin. The corpus callosum area was carefully dissected under high magnification in the dissecting microscope and used for obtaining white matter astrocytes. The tissues were rinsed with PBS containing 0.2% glucose (PBS/glucose); resuspended in PBS/glucose containing 10 mg/ml trypsin, 1 mg/ml DNase, and 5 mg/ml $MgSO_4$; incubated for 3 min at 37°C; and then carefully washed three times with PBS/glucose. After removal of the last wash solution, the tissues were suspended in DMEM containing 0.5 mg/ml DNase. Beginning with an 18-G needle, the tissues and the DNase solution were drawn up and expelled back in to the tube for a total of 15 times, and this procedure was repeated with the 20- and 23-G needles for 15 times each. The resulting cell suspension was centrifuged for 1 min at 1,200*g* for 1 min, and the pellet was resuspended in 1 ml of a 1:1 mixture of DNase solution and PBS/glucose/$MgSO_4$. The cell suspension was transferred onto the discontinuous Percoll gradient that had been made by overlaying 2.5 ml of 30% Percoll on 2.5 ml of 60% Percoll in PBS/glucose. After centrifugation at 1,200*g* for 10 min at 4°C, the astrocyte-enriched fraction that migrated to the medium/30% Percoll interface was carefully aspirated with a Pasteur pipette and suspended in 10 ml of PBS/glucose. The cells were centrifuged at 1,200*g* for 10 min at 4°C, resuspended in DMEM/10% FCS/3% glucose, plated at a concentration of 1×10^5 cells/ml in culture flasks (T25), and then cultured for at least 10 days. For subculturing or preparing for immunocytochemical and biochemical analyses, the cells were incubated with 0.05% trypsin/0.53 mM EDTA for 3 min at 37°C. After addition of an equal volume of DMEM/10% FCS, the cells were detached from the culture flasks by striking the side of the flasks, centrifuged, and resuspended in DMEM/FCS/glucose.

siRNA Transfecction

siRNA-mediated silencing of endogenous expression of S100A4 in astrocytes was performed according to a protocol (Kozlova and Takenaga, 2005). To silence S100A4, we used 21-nucleotide siRNA duplexes purchased from Ambion Inc. (Austin, TX). The sequence of sense and antisense oligo was 5′-GGGUGACAAGUUCAAGCUGtt-3′ and 5′-CAGCUUGAACUUGUCCACCCtc-3′, respectively. S100A4 siRNA (100 nM) was transfected with Lipofectamine 2000 according to the manufacturer's instructions. One day before transfection, astrocytes were resuspended in four-well plates in appropriate growth medium and then grown overnight on poly-L-lysine-coated coverslips. On the day of the experiment, siRNA-Lipofectamine 2000 complexes were prepared, and transfection was performed according to the manufacturer's instructions (Invitrogen, La Jolla, CA). The siRNA complexes were added dropwise while the four-well plates were gently rocked. Cells were transfected with S100A4 siRNA for at least 5 hr at 37°C before switching to fresh growth medium. As a control for S100A4 siRNA, Silencer Negative Control 1 siRNA (Ambion, Inc.) was used. After transfection, the medium was changed to DMEM supplemented with 3%glutamine, 10%fetal calf serum, and antibiotics. On day 3 after transfection, the DRGs were placed on the S100A4 siRNA- or control siRNA-transfected astrocytes. In experiments with extracellular S100A4, nontransfected white matter astrocytes from parallel cultures were treated with S100A4 protein in a con-

centration of 5 μg/ml 2 hr before DRGs were placed on the astrocytes.

DRG Cell Culture

We used transgenic green fluorescent protein (GFP) mice ubiquitously expressing GFP with a tau-tagged GFP transgene (Pratt et al., 2000). Adult GFP mice were anesthetized with 3.5% chloral hydrate (0.25 g/kg body weight), and DRG were removed, collected in Eppendorf tubes with 800 μl cold PBS, rinsed in another 800 μl portion of PBS, and transferred to 800 μl of 0.125% collagenase diluted in DMEM with 3% glutamine and with the addition of 10% FCS and antibiotics. DRGs with collagenase were incubated for 1 hr 20 min at 37°C in a humidified atmosphere with 5% CO_2. The collagenase solution was removed, and DRGs were resuspended in 500 μl DMEM and centrifuged for 5 min at 1,500 rpm. The supernatant was removed, and 500 μl fresh DMEM were added to the pellet, which was gently triturated. One hundred twenty-five microliters of DMEM containing 3×10^3 DRG neurons cells were added to each well with cultured astrocytes. The first group of astrocytes treated with control siRNA expressed high levels of S100A4. The second group of astrocytes was treated with S100A4 siRNA and was S100A4 negative. In the third group of astrocytes, recombinant human S100A4 (Tarabykina et al., 2000) was prepared as previously described (Novitskaya et al., 2000) and added at a concentration of 5 μg/ml 2 hr before DRGs were placed on top of the astrocyte cultures. Cytosine β-D-arabinofuranoside (Ara-C; Free Base/No. C1768; Sigma, St. Luois, MO) was applied to all cultures at a concentration of 0.05 mg/ml to the wells.

Microscopy

Coverslips with DRG-astroglial cocultures were examined and photographed in a Zeiss Axiovert S100 inverted fluorescence microscope 6, 12, 18, and 24 hr after seeding of DRG cells. In addition, coverslips were fixed at the same time points in 4% paraformaldehyde (w/v) and 14% saturated solution of picric acid (v/v) in 0.15 M phosphate buffer (pH 7.4) for 20 min, rinsed for 3 × 10 min with PBS, placed on slides, and mounted and examined in a microscope. To eliminate the risk of overlooking very thin neurites, which were common particularly after 12 hr of coculture, microscopic images were projected on the computer screen and the screen light was enhanced. Photographs were taken from 10 randomly placed frames on every coverslip.

Immunohistochemistry

After 6, 12, 18, and 24 hr of coculture, the coverslips from each group (control siRNA, S100A4 siRNA, and S100A4 treated) were placed on slides and incubated with primary antibodies: anti-glial fibrillary acidic protein (anti-GFAP; mouse monoclonal; 1:500; Jackson Immunoresearch, West Grove, PA), or anti-S100A4 (rabbit polyclonal; 1:700). Slides were incubated at 8°C overnight and thereafter rinsed three times with PBS and incubated with secondary antibodies: Texas red-conjugated donkey anti-mouse (1:80; Jackson Imunnoresearch) or Cy3-conjugated donkey anti-rabbit (1:500; Jackson Immunoresearch) for 4 hr at room temperature. The slides were rinsed three times with PBS and mounted in 50% glycerol in PBS containing 100 mM propylgallate to prevent photobleaching. Slides were examined in a Nikon Eclipse E800 microscope. For photography, a Nikon DXM1200F digital camera system was used.

Microscopic Analysis

For analyzing neurite outgrowth, we used a computer-based procedure developed by Rönn et al. (2000). Briefly, by means of the software package Process Length (Protein Laboratory), an unbiased counting frame containing a grid with a number of test lines was superimposed on the image. Twenty random images from each coverslip were made. The images were transferred to the Process Length program, and the number of intersections of cellular processes with the test lines was counted and related to the number of cell bodies for each image. In this way, the relative neurite length could be quantified. Each experiment was repeated at least three times.

Immunoblot

White matter astrocytes (3×10^5 cells) were seeded in 60-mm culture dishes. Sixteen hours later, the medium was changed to 2.5 ml of serum-free medium, and the cells were cultured for a further 24 hr. The conditioned medium (CM) was collected and concentrated 30-fold by using Centricon YM-3 (Amicon). An aliquot corresponding to 300 μl of the original CM and 25 ng of recombinant S100A4 (rS100A4) as a positive control were electrophoresed on 14% SDS-PAGE under reducing conditions. Proteins were electrophoretically blotted onto a Hybond-N membrane (Amersham Biosciences, Arlington Heights, IL). After blocking with 5% dry milk in TBS-T (150 mM NaCl, 50 mM Tris-HCl, pH 7.4, and 0.05% Tween 20), the membrane was incubated with affinity-purified anti-S100A4 antibody (1:500), washed extensively with TBS-T, and then with horseradish peroxidase-conjugated anti-rabbit IgG (1:3,000). Immunodetection of S100A4 was performed by using the enhanced chemiluminescence system (ECL; Amersham Biosciences).

RESULTS

DRG Cells on Poly-L-Lysine

We first determined the extent to which adult DRG cells developed neurites on poly-L-lysine in the absence of astrocytes. Adult DRGs showed good survival under these culture conditions but did not develop neurites during the 24-hr observation period (data not shown).

DRG Cell Neurite Outgrowth on Control siRNA-Treated Astrocyte Cultures

In the next series of experiments, we determined whether adult DRG cells developed neurites when cultured on white matter S100A4-expressing astrocytes. We examined the time course of neurite outgrowth on white matter astrocytes treated with control siRNA. These astrocytes expressed high levels of S100A4 but did not secrete S100A4 (Fig. 1). Six hours after coculture

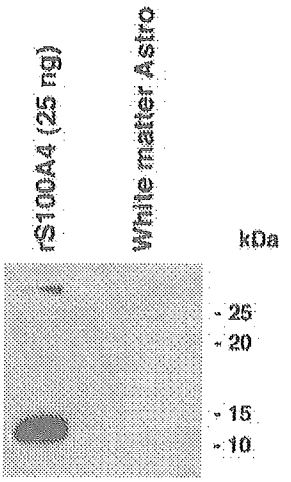

Fig. 1. S100A4 secretory property of white matter astrocytes. White matter astrocytes (3×10^5 cells/2.5 ml serum-free medium) were cultured for 24 hr. The conditioned medium was concentrated, and an aliquot was electrophoresed on 14% SDS-PAGE, followed by Western blotting. Recombinant S100A4 (rS100A4; 25 ng) served as a positive control. Immunodetection of S100A4 was performed with anti-S100A4 antibody.

with S100A4-expressing astrocytes, dissociated DRG cells had not extended fibers on astrocytes (Fig. 2A). Twelve hours after coculture, neurite growth from DRG cells was observed on S100A4-expressing astrocytes (Fig. 2B). After 18 hr of coculture with S100A4-expressing astrocytes, neurite growth from DRGs was increased. After 24 hr of coculture, strong neurite growth was recorded on S100A4-positive astrocytes (Figs. 2C, 3A). These findings show that cultured white matter astrocytes support neurite outgrowth from adult DRG cells.

DRG Cell Neurite Outgrowth on S100A4 siRNA-Treated Astrocyte Cultures

To explore the role of intracellular S100A4, we examined DRG cell neurite outgrowth on white matter astrocytes treated with S100A4 siRNA. Three days after this treatment, the expression of S100A4 is almost completely eliminated (Takenaga and Kozlova, 2005). At this time, dissociated adult DRG cells were placed on the astrocytes. Six hours after coculture with S100A4-silenced astrocytes, no neurite outgrowth from DRG neurons was recorded. Twelve hours after coculturing, extensive neurite growth from dissociated DRG cells was recorded. Eighteen hours after coculture, the neurite growth from DRG neurons was increased on S100A4-negative astrocytes (Fig. 3B), with an additional increase 24 hr after coculturing of DRG neurites. The quantitative analysis showed that neurite outgrowth at 12, 18, and 24 hr was significantly greater in S100A4 siRNA-treated compared with control siRNA-treated cultures (Figs. 4, 5). These findings indicate that down-regulation of S100A4 expression in white matter astrocytes promotes neurite outgrowth from adult DRG cells.

DRG Cells on S100A4-Treated S100A4-Expressing Astrocyte Cultures

To determine whether extracellular S100A4 protein influences DRG neurite outgrowth on white matter astrocytes, we prepared white matter astrocyte cultures and added recombinant S100A4 protein (5 μg/ml) to these cultures 2 hr before dissociated adult DRG cells were seeded on top of the astrocytes. This concentration has previously been shown to provide maximal neurite outgrowth in vitro (Novitskaya et al., 2000; Pedersen et al., 2004). Six hours later, no neurite growth was recorded. Twelve hours after coculture, long neurites extended from the DRG neurons. At 18 hr in culture, extreme neurite outgrowth was observed on S100A4-expressing astrocytes (Fig. 4C). After 24 hr in culture, the growth of DRG fibers was still extensive (Fig. 5). The quantitative analysis showed significantly greater neurite outgrowth in S100A4-treated cultures compared with control siRNA cultures at 12, 18, and 24 hr as well as S100A4 siRNA-treated cultures at 18 hr (Figs. 4, 5). Thus, in contrast to intracellular S100A4, extracellular S100A4 stimulates neurite outgrowth.

DISCUSSION

Our main findings are that white matter astrocytes are able to support neurite growth from adult DRG cells and that S100A4 protein, a constitutive component of white matter astrocytes, has opposite effects on neurite growth depending on whether the protein is expressed intracellularly or provided extracellularly. Astrocytes react to direct injury to the CNS and are the predominant cell type in the glial scar. Reactive astrocytes also play a predominant role at the junction between the peripheral and the central nervous systems in preventing regenerating dorsal root axons from entering the spinal cord. In both instances, astrocytes produce factors that are inhibitory for axonal regeneration (for review see Silver and Miller, 2004; Carulli et al., 2005). Our observations, therefore, are relevant generally in the context of the interaction between reactive white matter astrocytes and growth of injured CNS axons. Given that we explored neurite growth from adult DRG cells, our observations are particularly relevant with regard to the interactions between regenerating dorsal root axons and astrocytes at the dorsal root entry zone.

White matter astrocytes were found to support neurite growth from adult DRG cells. This finding is in line with previous findings that adult DRG cells are able to extend lengthy neurites on organotypic slice cultures of postnatal day 35 rat brain containing the corpus callosum (Tom et al., 2004). Because extracellular S100A4 is neuritogenic in vitro, this growth support could be a result of S100A4 secretion. However, we found no evidence for S100A4 protein in immunoblot analysis of medium from S100A4-expressing white matter cultures.

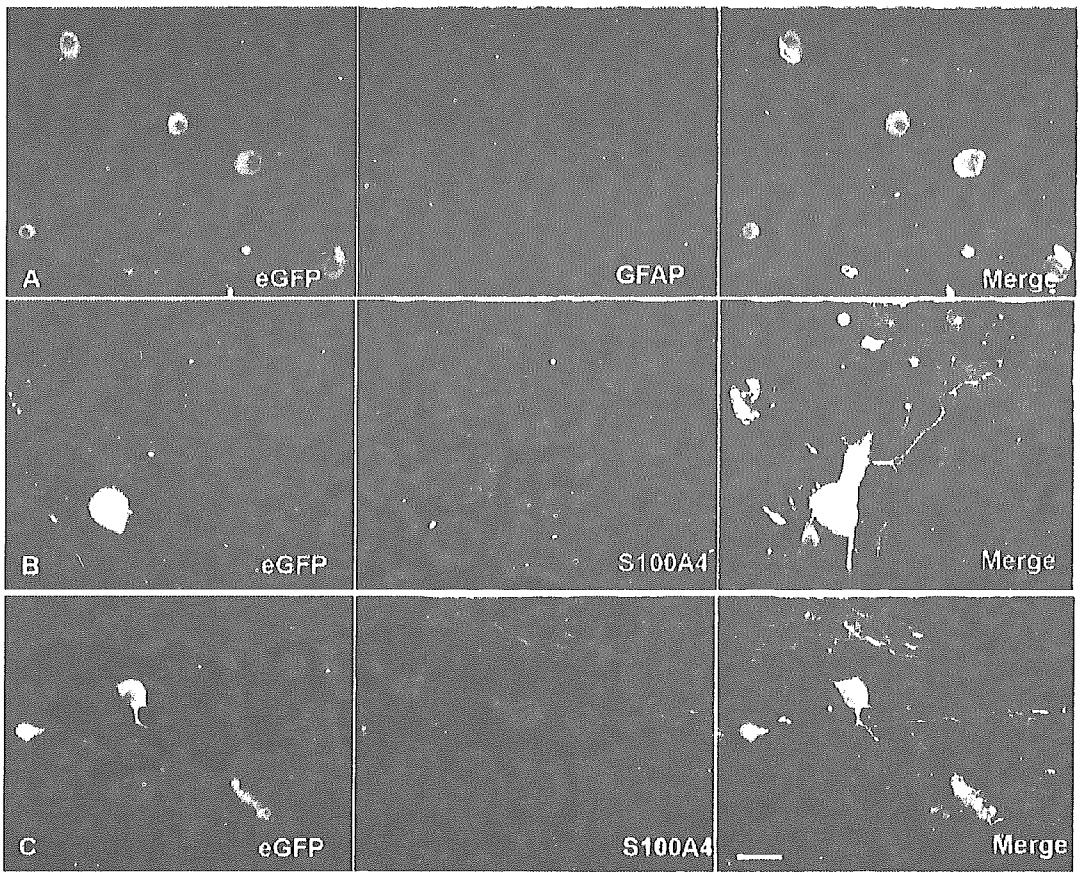

Fig. 2. Neurite growth from GFP-expressing dorsal root ganglion cells 6, 12, and 24 hr after seeding on cultures of white matter control siRNA-treated astrocytes. No neurites are visible 6 hr after seeding (**A**). From 12 (**B**) to 24 (**C**) hr, there is a marked increase in neurite outgrowth. The middle panel shows labelling of astrocytes with antibodies to glial fibrillary acidic protein (GFAP; A) and S100A4 (B,C). The right panel shows merged pictures of GFP/antibody labelling. Scale bar = 50 μm.

Intracellular S100A4 had an inhibitory effect on the potential of white matter astrocytes to support neurite growth, in that siRNA-mediated down-regulation of S100A4 expression resulted in a significant increase in DRG neurite outgrowth. By using the same technique, we previously showed that down-regulation of intracellular S100A4 in white matter astrocytes increases their migration in a transwell migration assay (Takenaga and Kozlova, 2005). Furthermore, this increased migration was associated with an increased synthesis and activity of metalloproteinases MT1-MMP and MMP-9. The increased motility of white matter astrocytes and a change in extracellular metalloproteinase activities are, therefore, two factors that may promote DRG neurite outgrowth on S100A4-silenced astrocytes. Conversely, the reduced neurite outgrowth on S100A4-expressing white matter astrocytes may be a consequence of reduced motility and/or down-regulation of metalloproteinase synthesis in these cells. This influence of S100A4 on MMPs may be important for axon growth in the CNS, insofar as the balance between the activity of metalloproteinases and their inhibitors is crucial for the possibilities for cells and processes to negotiate the CNS white matter (Belien et al., 1999; Gardner and Ghorpade, 2003; Ahmed et al., 2005) as well for regeneration of peripheral nerve axons (Krekoski et al., 2002; Shubayev and Myers, 2004).

We find that, in contrast to the inhibitory influence of intracellular S100A4, extracellular S100A4 promotes DRG neurite growth on white matter astrocytes, to an extent that surpasses the growth observed on S100A4-silenced white matter astrocytes. This outgrowth may be mediated by a direct effect on the DRG neurons and/or indirectly via an effect on the S100A4-expressing astrocytes.

Results from previous studies show that extracellular S100A4 is a potent neurite outgrowth-stimulating factor on embryonic hippocampal and mesencephalic, as well as early postnatal cerebellar neurons in vitro (Novitskaya et al., 2000; Pedersen et al., 2004). Our findings provide a basis for further generalization of extracellular S100A4 as a neuritogenic factor. The mechanisms underlying the growth-promoting effect of extracellular